Title

Rhesus macaque versus rat divergence in the corticospinal projectome

Journal

Neuron, 110(18)

ISSN

0896-6273

Authors

Sinopoulou, Eleni

Rosenzweig, Ephron S

Conner, James M

et al.

Publication Date

2022-09-01

DOI

10.1016/j.neuron.2022.07.002

Peer reviewed

HHS Public Access

Author manuscript

Neuron. Author manuscript; available in PMC 2023 September 21.

Published in final edited form as:

Neuron. 2022 September 21; 110(18): 2970–2983.e4. doi:10.1016/j.neuron.2022.07.002.

Rhesus Macaque vs. Rat Divergence in the Corticospinal Projectome

Eleni Sinopoulou[1,*], **Ephron S. Rosenzweig**[1,*], **James M. Conner**[1,†], **Daniel Gibbs**[1,†], **Chase A. Weinholtz**[1], **Janet L. Weber**[1], **John H. Brock**[1,2], **Yvette S. Nout-Lomas**[3], **Eric Ovruchesky**[1], **Yoshio Takashima**[1], **Jeremy S. Biane**[1], **Hiromi Kumamaru**[1], **Leif A. Havton**[4], **Michael S. Beattie**[5], **Jacqueline C. Bresnahan**[5], **Mark H. Tuszynski**[1,2]

[1]Dept. of Neurosciences, University of California - San Diego, La Jolla, CA

[2]Veterans Administration Medical Center, La Jolla, CA

[3]College of Veterinary Medicine and Biomedical Sciences, Colorado State University, Fort Collins, CO

[4]Departments of Neurology and Neuroscience, Icahn School of Medicine at Mount Sinai, NY, NY, Veterans Administration Medical Center, Bronx, NY

[5]Dept. of Neurosurgery, University of California, San Francisco, CA

SUMMARY

We used viral intersectional tools to map the entire projectome of corticospinal neurons associated with fine distal forelimb control in Fischer 344 rats and rhesus macaques. In rats, we found an extraordinarily diverse set of collateral projections from corticospinal neurons to 23 different brain and spinal regions. Remarkably, the vast weighting of this “motor” projection was to *sensory* systems in both the brain and spinal cord, confirmed by optogenetic and trans-synaptic viral intersectional tools. In contrast, rhesus macaques exhibited far heavier and narrower weighting of corticospinal outputs toward spinal and brainstem *motor* systems. Thus, corticospinal systems in macaques primarily constitute a final output system for fine motor control, whereas this projection in rats exerts a multi-modal integrative role that accesses far broader CNS regions. Unique

Correspondence to: Mark H. Tuszynski, Dept. Neurosciences, 0626, University of California, San Diego, La Jolla, CA 92093, 858-534-8857, 858-534-5220 (fax), mtuszynski@ucsd.edu.

†Current affiliation: Salk Institute for Biological Studies, La Jolla, CA

*Contributed equally to this work

Lead Contact

Further information and requests for resources and reagents should be directed to Mark Tuszynski (mtuszynski@health.ucsd.edu)

Author contributions:

ES, ESR, JMC, DG, YT, JSB, HK, LAH, MSB, JCB, and MHT designed experiments.

ES, ESR, JMC, YSN-L, YT, JSB, and MHT performed surgery.

ES, JMC, CAW, JLW, EO, YT, JSB, and HK processed tissue.

ES, ESR, JMC, DG, CAW, JLW, EO, YT, JSB, and HK imaged tissue.

ES, ESR, JMC, DG, CAW, EO, YT, JSB, HK, and MHT analyzed data.

ES, ESR, JMC, DG, MSB, JSB and MHT wrote the manuscript.

ES, ESR, JMC, DG, CAW, JLW, YSN-L, EO, YT, JSB, HK, LAH, MSB, JCB, and MHT edited the manuscript.

The authors declare no competing interests.

structural-functional correlations can be achieved by mapping and quantifying a single neuronal system's *total* axonal output and its relative weighting across CNS targets.

Keywords

Spinal cord; motor cortex; motor control; corticospinal; viral tracing; trans-synaptic tracing; optogenetics; imaging; projectome mapping; neural circuits; rhesus macaque; monkey

INTRODUCTION

Skilled motor behavior is a critical evolutionary adaptation of mammalian species and reflects neuronal processing and integration across a highly distributed network. Primary motor cortex constitutes a key part of this distributed network and serves as the site for planning, initiating, and orchestrating complex voluntary movements (Canedo, 1997; Kalaska, 2009; Alstermark and Isa, 2012; Georgopoulos and Carpenter, 2015). A key feature of this circuitry is the descending output arising from layer V neurons in primary motor cortex that project to the spinal cord and influence the activation of peripheral musculature (Canedo, 1997; Alstermark and Isa, 2012).

While direct cortical projections to the spinal cord likely play a key role in mediating motor control, corticospinal neurons also send "copies" of presumptive motor commands and predicted sensory responses to other brain structures via axon collaterals (Phillips and Porter, 1977; Adams et al., 2013; Azim et al., 2014). These axon collateral "efference copies" are postulated to play important roles in the modulation of motor output via cerebellar feed-forward models (Miall and Wolpert, 1996; Scott, 2004; Shadmehr et al., 2010; Azim and Alstermark, 2015) and for anticipating and cancelling the sensory effects of self-generated movements (Blakemore et al., 2000; Cullen, 2004; Crapse and Sommer, 2008). While the existence of corticospinal collaterals associated with efference copies has been previously documented (Canedo, 1997; Parent and Parent, 2006; Hattox and Nelson, 2007; Lemon, 2008; Kita and Kita, 2012), prior studies have not defined the *weighting* of these corticospinal collaterals to different structures and their post-synaptic targets. Moreover, collateralization and connectivity of neuronal architecture arising from *functionally defined* subpopulations of corticospinal neurons, such as those involved in skilled grasping, have not been assessed previously. Recently-developed intersectional viral tools now make it possible to comprehensively map in an unbiased manner all outputs and, in some cases, trans-synaptic targets of specific neuronal sub-types in non-transgenic species (Fig 1A; see also Petreanu et al., 2007; Lo and Anderson, 2011; Schwarz et al., 2015).

Using these tools in non-transgenic rats and rhesus macaques, we sought to define the complete corticospinal projectome involved in distal forelimb motor control in two divergent species. The resulting data deeply inform structural/functional correlates of motor control within each species. Furthermore, comparison across species reveals important evolutionary specializations that are associated with increasingly fine motor control (Leonelli, 2012; Lemon, 2019), and also addresses the relevance of rat models to predicting impacts of treatments after spinal cord injury in primate species.

RESULTS

Rat Studies

In Fischer 344 rats, an intersectional viral approach was used to express genetically encoded axonal tracers, optogenetic actuators, or anterograde trans-synaptic tracers specifically in corticospinal neurons associated with distal forelimb motor control (Fig 1A). To selectively express Cre in corticospinal neurons projecting to lower cervical spinal cord, and enable their subsequent genetic manipulation, AAV9-CaMKII-Cre was targeted bilaterally to the C7-T1 spinal cord segments (n=4 rats). This approach provided an efficient means of retrogradely infecting corticospinal neurons with Cre from their terminal projections (Masamizu et al., 2011; Elmallah et al., 2012; Cook-Snyder et al., 2015; Green et al., 2016; Biane et al., 2019). To subsequently define the full pattern of axonal projections arising from this specific corticospinal population, AAV vectors expressing Cre-dependent, membrane bound tracers (AAVDJ-FLEX-ArchT-TdTomato or AAV8-FLEX-HM4D-mCherry) were injected into the forelimb area of the primary motor cortex (Fig 1C). As a result, we expressed membrane-localized fluorophores exclusively in layer V corticospinal neurons projecting to the spinal segments (C7-T1) associated with distal forelimb function (Fig 1 C, D). This approach enabled highly sensitive labeling and subsequent quantification of all collateral branches arising from distal forelimb-projecting layer V corticospinal motoneurons throughout the brain, brainstem, and spinal cord (Fig 1B and Supp. Fig 1A). To compare the comprehensive outputs of the corticospinal projection across species, we calculated percentage innervation of each brain region per animal compared to the total output of the corticospinal projection in the same animal. This approach also normalized for any differences in the efficiency of fluorescent labeling in each subject.

Rat Corticospinal Axons Project Throughout the Brain

Results obtained using this paradigm identify a remarkably widespread and unprecedented set of projections arising from a single, functionally-restricted subset of corticospinal neurons influencing distal forelimb function (Fig 1B and Supp. Fig 1A). A mean of 685 ± 154 layer V corticospinal neurons were labelled among these 4 rats, and all observed neuronal cell bodies were present in layer V of M1 (Fig. 1D). Collaterals of C7-T1-projecting layer V corticospinal neurons are observed in 16 distinct supratentorial and brainstem regions, not including their projections to the spinal cord. In addition to previously identified collateral targets of corticospinal projections such as the somatosensory cortex (4.0 ± 0.2%, Fig 2A) (Deschênes et al., 1994; Lévesque et al., 1996; Canedo, 1997), we also identify novel projections to multiple basal ganglia targets (Fig 2B), the lateral globus pallidus and entopeduncular nucleus (internal globus pallidus), and multiple thalamic nuclei (Supp. Fig. 1A, 2A).

An important feature of this intersectional approach for axonal projection mapping was the ability to quantify the relative *weighting* of corticospinal innervation across different brain and spinal cord regions; this provided the total projectome arising from the subset of corticospinal neurons associated with distal forelimb motor control. Notably, more than half (55%) of the entire rat corticospinal projectome associated with distal forelimb motor control actually terminates *rostral to* the spinal cord in several supratentorial and brainstem

structures, with the output distributed almost equally across basal ganglia, sensory, and motor targets (Fig 1B and Supp. Fig 1A). The most heavily innervated supratentorial structures were the ipsilateral striatum, which received 16.7 ± 0.8% of corticospinal total axonal output (Fig 2B), the zona incerta and subincerta (Fig 2C), which received 8.5 ± 0.8% of corticospinal output, followed by the somatosensory cortex (4.0 ± 0.2%; Fig 2A) and the thalamus (3.1 ± 0.1%; Fig 2D). Supratentorial targets accounted for 34.4 ± 1.6% of all corticospinal output arising from neurons controlling the distal digits.

The brainstem received a total of 20.7 ± 1.9% of total corticospinal axonal output related to distal forelimb control. The densest brainstem projection was to the gigantocellular tegmental nucleus (6.5 ± 1.4%; Fig 2E), a portion of the medullary reticular formation that is involved in motor control (Lemieux and Id, 2019). The next most dense input was to a purely sensory nucleus that receives proprioceptive input from the cervical spinal cord, the cuneate nucleus (3.3 ± 0.4%; Fig 2F). This was followed by the pontine nucleus (3.3 ± 0.04; Fig 2G), a relay projection to the cerebellum, and the red nucleus (2.6 ± 0.2%; Fig 2H), a motor projection to the spinal cord. There were also projections to the anterior pretectal nucleus (2.2 ± 0.2% Fig 2I) and the periaqueductal gray (1.2 ± 0.3% ; Fig 2J). Synaptic transmission was confirmed in several of these regions, including the striatum (Fig. 2K–M), using optogenetics as discussed in greater detail below.

Corticospinal Projections to the Spinal Cord

A total of 43.9 ± 2.3% of total corticospinal output related to distal forelimb control terminated in the spinal cord (Fig 1B, Fig 3 A–E). Notably, however, the densest projection was to the *upper* cervical spinal cord (C1–5; 27.7 ± 1.5%; Fig 3A, B, E) rather than the *lower* cervical spinal cord (Fig 3A–D), despite the fact that mapping was initiated by injection of retrograde *cre* injections into spinal cord segments C7-T1. Indeed, only 13.8 ± 1.0% of the output of corticospinal neurons controlling the distal forelimb project to the *lower* cervical spinal cord. Thus, the vast collateral network of corticospinal axons related to distal forelimb control terminates primarily in the *upper* cervical spinal cord, the supratentorial compartment and brainstem structures. As expected, the densest corticospinal terminal region in both upper and lower cervical spinal cord regions was within Rexed's lamina 5–7, with only sparse innervation of deeper laminae 8–9 (Fig 3 and Supp. Fig 3A). Lumbar collaterals of corticospinal axons related to distal forelimb control were virtually absent (Fig 1B and Supp. Fig 4A). 92.9 ± 0.1%of corticospinal inputs to the spinal cord terminated contralateral to the hemisphere of origin (Fig 1B and Fig 3E).

Anterograde Trans-synaptic Tracing Shows Extensive Corticospinal Access to Sensory Processing Centers in the Spinal Cord

To more deeply identify connectivity patterns of corticospinal projections involved in distal forelimb control, we mapped their trans-synaptic projections using a cre-dependent anterograde trans-synaptic tracer, HSV129-TK-TT (Lo and Anderson, 2011). Retrogradely transported cre virus was injected into C7-T1 spinal segments as described above, and cre-dependent HSV129-TK-TT was injected into primary motor cortex,thereby driving HSV spread specifically from corticospinal neurons associated with distal forelimb control (N=5 animals). After 2–4 days, a time sufficient to allow postsynaptic virus spread, the majority

of neuronal labeling in the spinal cord was restricted to sites containing axon collaterals of C7-T1-projecting corticospinal neurons, suggesting that many of these cells were either mono- or di-synaptic targets of corticospinal neurons (Fig 3B, C, E).

HSV129-TK-TT spread trans-synaptically (likely disynaptically) to alpha motoneurons only within the lower C6-T1 spinal cord segments (Fig 3C); however, within upper cervical segments HSV129-TK-TT spread into trans-synaptic target circuits in *dorsal* spinal gray matter regions associated with sensory processing (Fig 3C) rather than ventral motoneuron pools. Quantification of the relative density of trans-synaptic labeling in ventral, central and dorsal gray matter of lower vs. upper cervical segments showed that lower cervical spinal cord segments received more than 4-fold greater proportional polysynaptic corticospinal spread to ventral gray matter compared to upper cervical segments (Supp. Fig 5D). Numerous trans-synaptically labeled cells were also present, across all spinal segments, in the internal basilar nucleus (which contains somatosensory relay neurons of the spinothalamic tract) (Huang, 1989), as well as in other dorsal sensory regions (Fig 3C). This restriction of alpha motoneuron labeling to lower cervical segments is consistent with the hypothesis that ultimate synaptic communication of a distal forelimb motor command uniquely reaches lower motoneuron pools in spinal segments associated with distal forelimb control, and that copies of that motor command are integrated with multiple sensory and motor processing streams throughout the rest of the cervical spinal cord. (We did not quantify either the number of “starter” cells in the cortex initially infected with HSV or the number of post-synaptic targets in the spinal cord because HSV spreads to across synapses rapidly and poly-synaptically, making quantification of indeterminate value).

Trans-Synaptic Motor Interneuronal Targets of Corticospinal Neurons in the Spinal Cord

We further characterized the mono- and poly-synaptic targets of corticospinal terminals in upper and lower cervical spinal cord segments using a panel of cell type-specific neuronal markers for spinal ‘motor interneurons’ (spinal interneurons that access motor circuits). Notably, in the lower cervical spinal cord (the level from which all intersectional neuronal labeling was *initiated* with retrograde delivery of Cre recombinase) we observed co-localization of mono- and polysynaptic HSV-TdTomato with Ap2b-labeled motor synergy encoder (MSE) neurons (Levine et al., 2014) (Fig 3D, Supp. Fig 5A), ChAT-labeled V0c neurons in central gray (Zagoraiou et al., 2009) (Fig 3D, Supp. Fig 5B), Chx10-labeled V2a motor interneurons (Briscoe et al., 2000; Ericson et al., 1997) (Fig 3D), and as noted above, ChAT-labeled alpha motoneurons (Fig 3D, Supp. Fig 5C). These parallel a classic set of spinal motor targets of corticospinal terminals identified in mouse neural development (Ericson et al., 1997; Briscoe et al., 2000; Zagoraiou et al., 2009). In the upper cervical spinal cord, collaterals from the same corticospinal network innervated circuits containing Ap2b-expressing motor interneurons in the deep medial dorsal gray (Levine et al., 2014); however, no neurons at upper cervical levels co-localized with Chx10-expressing V2a motor interneurons, ChAT-expressing alpha motor or ChAT-expressing V0c neurons, consistent with a projection pattern in the upper cervical spinal cord that primarily targets sensory processing. Thus, layer 5 corticospinal neurons projecting to the spinal cord access distinct post-synaptic circuits at upper vs. lower levels of the spinal cord, with a bias toward *motor* networks in spinal segments controlling the distal forelimb. (Precise quantification of

post-synaptic targets of corticospinal axons in the spinal cord is not provided due to potential HSV-mediated neuronal loss and differential rates of trans-synaptic spread among distinct neuronal subclasses, making quantification of uncertain value.)

In addition to employing the anterograde *poly-synaptic* HSV129-TK-TT tool to trace targets of corticospinal inputs to the spinal cord, we also employed a second anterograde *mono-synaptic* tracer in rats that takes advantage of relatively weak anterograde trans-synaptic transport of AAV1 vectors. A Cre-dependent TdTomato vector was injected into spinal cord segments C7-T1 (AAVDJ-Flex-ArchT-TdTomato), and a Cre vector (pAAV1-hSyn1-ddCre) was injected into the forelimb region of the motor cortex. At high titers, AAV1 crosses into the postsynaptic neuron (Zingg et al., 2017). Anterograde trans-synaptic transport of Cre from corticospinal neuron terminals in the spinal cord resulted in labeling of corticospinal partner neurons in the spinal cord with TdTomato. This technique revealed that monosynpatic partners of corticospinal neurons were primarily located in medial dorsal and medial intermediate gray matter regions; virtually no mono-synaptic projections to spinal alpha motoneurons were detected in either rostral or caudal spinal cord segments, as expected. Quantification of mono-post-synaptic partners of corticospinal projections in the cervical spinal cord revealed that 98.3 ± 4.8% of the collateral projections terminated in interneurons. Projections to inhibitory interneurons of the intermediate zone were also identified, and accounted for 17.9 ± 2.3% of the total amount of all collateral projections to interneurons in the rat (Supp. Fig 6A, C, E).

Optogenetic Tools Confirm the Presence of Functional Synapses

We confirmed physiological activity of several corticospinal collateral projections using optogenetic tools (Fig 2K–M and Supp. Fig 7), including the striatum and anterior pretectal nucleus. The intersectional viral strategy was used to express channelrhodopsin-2 specifically in C7-T1-projecting corticospinal neurons within the rat primary motor cortex. A total of 10 animals were used for these experiments and received injections of both the AAV9-CamKII-Cre virus into C7-T1 spinal cord segments and AAV8-FLEX-ChR2-GFP (UNC Vector Core) virus into the motor cortex. Three weeks later, brain slices were prepared and in vitro whole cell patch techniques were used to record light-evoked responses of corticospinal terminals containing ChR2 (Petreanu et al., 2007; Cruikshank et al., 2010; Biane et al., 2016). In every innervation region tested, postsynaptic responses could be evoked optogenetically. Monosynaptic connections were confirmed in a subset of these targeted structures using bath application of tetrodotoxin (TTX) and 4-aminopyridine (4-AP; Fig 2K–M and Supp. Fig 7; Petreanu et al., 2007, 2009). Monosynaptic inputs were confirmed in striatal (Fig 2L–M) and anterior pretectal structures (Supp. Fig 7).

In summary, rat studies of corticospinal neurons associated with distal fine motor control revealed an extensive system of collateral projections throughout the brain and spinal cord. Remarkably, only 13.8 ± 1.0% of axons extending from this class of corticospinal neuron terminate in lower spinal cord segments. The vast majority of this corticospinal output accesses sensory and motor control centers in the spinal cord, brainstem, thalamus and striatum, likely exerting a role in integrating and modulating fine motor output.

PRIMATE STUDIES

In rhesus macaque monkeys, a similar intersectional viral approach was used to specifically deliver genetically encoded axonal tracers to corticospinal neurons associated with distal forelimb motor control (Fig 4A). An AAV vector optimized for retrograde transport (AAVrg) expressing Cre (AAVrg-pmSyn1-EBFP-Cre) was injected into right C7-T1 spinal cord segments (n=4 adult rhesus monkeys), and an AAV vector expressing a modified form of GFP enhanced for membrane trafficking (AAVdj-CAG-DIO-gCOMET) was injected into the left primary motor cortex forelimb region (Fig 4C, D) (see Methods). As a result, membrane-localized fluorophores were expressed exclusively in layer V corticospinal neurons projecting to the spinal segments (C7-T1) associated with distal forelimb function (Fig 4D). As in rat studies, this approach enabled highly sensitive and specific labeling along with objective quantification of all collateral axon branches arising from these neurons throughout all supratentorial areas, the brainstem and the spinal cord (Fig 4B and Supp. Fig 1B).

Macaque Corticospinal Axon Collaterals in the Brain are Sparse Compared to the Rat

Compared to the rat, in which a total of 34.4 ± 1.6% of the total axonal output of the corticospinal system terminated supratentorially, significantly fewer rhesus macaque corticospinal projections, 6.8 ± 2.0%, terminated in supratentorial areas (Fig 5A). This difference was highly significant ($t6_{,\ 10.65}$, $p<0.0001$, two-tailed t-test; Fig 5A). Most supratentorial collaterals in the rhesus macaque projected to the ventral anterior and ventrolateral nuclei of the thalamus 3.3 ± 1.2% (Fig 4B, Fig 5B and Supp Fig 2B,C). In contrast to the rat, striatal projections were minimal (0.3 ± 0.1%) in rhesus macaque, a difference that was statistically significant ($t6_{,\ 6.808}$, $p=0.0005$, two-tailed t-test; Fig 4B). Corticospinal axons projecting to these regions co-labeled with synaptophysin (Supp. Fig 8).

Brainstem Projections

Projections of the corticospinal system to the brainstem in the rhesus macaque constituted 18.9 ± 0.1%of all corticospinal projections associated with distal forelimb control (Fig 5C–H). The most abundant corticospinal projection to the brainstem targeted the pontine nucleus (18.7 ± 2.5%, Fig. 5C–D). There were modest projections to the red nucleus (1.7 ± 0.5%; Fig 5E), the lateral reticular nucleus (1.6 ± 0.5%), and the pedunculopontine tegmental nucleus (0.9 ± 0.4%;Fig 5F–G). In contrast to the rat, virtually no corticospinal collaterals in the macaque projected to the cuneate nucleus (0.1 ± 0.1% ; Fig 5H). Overall, total proportionate outputs of corticospinal projections associated with distal forelimb control to the brainstem were similar in the macaque and rat (18.9 ± 0.1% and 20.7 ± 1.9%, respectively; Fig 5A).

Corticospinal Outputs Primarily Reach the Spinal Cord in Macaques

In macaques, the vast bulk of corticospinal axonal projections related to distal forelimb control projected to the spinal cord: 67.1 ± 0.1% (Fig. 5A). Of these spinal cord projections, the greatest projections were to spinal cord segments C6-T1 (Fig. 4B, Fig 6A, G), comprising 35.5 ± 0.1% of the entire corticospinal projection. In the rat, only 13.8 ± 1.0% of the corticospinal projection termined in the lower cervical spinal cord, and 43.9 ± 2.3%

to the spinal cord overall. Thus, the corticospinal network related to control of the distal forelimb is far more greatly weighted toward direct spinal cord inputs. Most corticospinal terminals in the macaque were located in intermediate spinal gray matter (Fig 6A, Supp. Fig. 3B). Moreover, there were more bilateral corticospinal projections to the spinal cord in monkeys, with 7.1 ± 0.1% of corticospinal axons terminating in the spinal cord ipsilateral to the cortex of origin (Fig 6A). There was no detectable innervation of the lumbar spinal cord from corticospinal axons projecting to the distal forelimb (Supp. Fig 4B).

Trans-Synaptic Targets of Corticospinal Neurons in the Spinal Cord

We performed anterograde trans-synaptic labeling to identify the *monosynaptic* partners of corticospinal projections to the spinal cord in two monkeys (Fig 6B). This was accomplished by injections of Cre-dependent TdTomato into spinal cord segments C7-T1 (AAVDJ-Flex-ArchT-TdTomato) and injections of a Cre vector (pAAV1-hSyn1-ddCre) into the forelimb region of the motor cortex, as noted above, taking advantage of weak anterograde transsynaptic AAV1 transport in the nervous system (Zingg et al., 2017). 81% of neurons trans-synaptically labeled in the spinal cord of monkeys were alpha motoneurons located in lamina IX motoneuron pools: (436 of 574 neurons in monkey 1 and 208 or 243 neurons in monkey 2; Fig 6C,D and Supp. Fig 6B). The remaining 19% of trans-synapatically labelled cells were interneurons located in laminae V-VIII and X (138 of 574 neurons in monkey 1 and 35 of 243 neurons in monkey 2). Of these interneurons in lamina V-VIII and X, 29.3%± 1.7% co-localized with parvalbumin, a marker of inhibitory neurons (Fig 6F and Supp. Supp. Fig 6B,D), and 53.6 ± 0.3% with ChAT, a marker of V0c excitatory interneurons (Fig 6E). Corticospinal axons did not project onto Satb1 interneurons (Supp. Fig 9), in contrast to findings in rats. Thus, the majority of corticospinal axons related to distal forelimb control in rhesus macaques directly access alpha motoneurons.

DISCUSSION

We have for the first time in rats and rhesus macaque mapped the entire collateral axonal network of corticospinal neurons that modulate distal forelimb control. The quantification of projections was unbiased, based on intersectional viral labeling techniques that allowed a calculation of the quantitative “weight” of corticospinal collateral output to individual regions of the entire neuraxis. Further, the viral intersectional toolkit allowed us to precisely map the organization of not just the general corticospinal system, but the specific component of the system focused on distal forelimb control, arguably the most important and highly evolved motor function in humans. The resulting findings identify extensive differences in the topography, weighting, and function of corticospinal systems in rodent vs. primate species (Fig 7).

In rats, the majority of the corticospinal system projects to sensory and sensorimotor integrative centers, including the striatum, sensory thalamic nuclei, the brainstem, *upper* cervical spinal cord sensory regions and lower spinal cord motor centers. In contrast, the macaque corticospinal system related to distal forelimb control is far more heavily weighted to motor systems: the greatest proportional projection is to the lower cervical spinal cord. There is also, consistent with previous work (Hoff and Hoff, 1934; Liu and Chambers, 1964;

Kuypers and Brinkman, 1970; Jankowska et al., 1975; Bortoff and Strick, 1993; Lacroix et al., 2004; Rosenzweig et al., 2009) greater *bilateral* projection of the macaque corticospinal system to the spinal cord. 98% of *synaptic boutons* have been identified as terminating contralaterally (Morecraft et al., 2013). Macaque corticospinal collateral projections to the brain are much more limited than in the rat, and even these are directed to motor control regions of the thalamus; there is almost no striatal projection. Similarly, macaque corticospinal collateral projections to the brainstem are primarily to motor control systems.

The viral intersectional tools used in this study generate a new depth of understanding regarding the role of corticospinal projection systems for hand control in the rat and macaque. While many but not all of the targets of corticospinal output identifed in this study have been previously appreciated (Akintunde and Buxton, 1992; Parent and Parent, 2006; Hattox and Nelson, 2007; Kita and Kita, 2012b), knowledge of the proportional distribution of corticospinal collaterals to each target region has been entirely lacking. By revealing the proportionate weighting of the entire corticospinal projectome related to hand control, one can appreciate that In the rat the corticospinal system is clearly a sensorimotor integrator, as the majority of its output reaches sensory systems, as described above. This confirms previous hypotheses that “efference copies” of corticospinal projections to sensory systems exert a role in modulating motor output in *rats and mice* (Shadmehr et al., 2010; Abraira and Ginty, 2013; Azim and Alstermark, 2015; Nelson et al., 2021). However, in rhesus macaques mapping of the corticospinal projectome related to hand control reveals that the entire system is far more narrowly focused on motor outputs and, by inference, fine motor control. Integration of sensory and motor systems remains critical to motor function in both species, but these two systems are more segregated and specific in their projection patterns among primates that exhibit exquisite motor dexterity.

Using intersectional trans-synaptic tools for mapping anterograde targets of corticospinal projections in both species, we now readily appreciate that corticospinal projections in rats primilary access sensory systems while macaque projections heavily access motor systems. Moreoever, trans-synaptic targets of corticospinal projections have been previously mapped in transgenic mice (Levine et al., 2014) but not in rats or macaques; we now identify these targets in both species. As in mice, trans-synaptic targets of corticospinal projections in rats consist of Ap2b motor synergy encoder (MSE) neurons, V2a motor interneurons, and V0c motor interneurons. However, in macaques the most abundant trans-synaptic targets of corticospinal projections are alpha motor neurons, followed by V0c motor interneurons and inhibitory (parvalbumin-labeled) interneurons.

A recent study in mice also used intersectional methods to map the corticospinal projectome, but did not include spinal cord outputs in its analysis (Nelson et al., 2021). This elegant study identified a major output of corticospinal projections to the striatum that exert a role in encoding information related to the onset and offset of motor synergies. Such a role likely also exists in the rat: we find that the striatum is the third most abundant recipient of corticospinal inputs related to distal forelimb motor control. Notably, however, the striatum is a very minor target in the rhesus macaque, highlighting distinctions in the functional neuroanatomy of corticospinal systems between rodents and primates. There were also differences in projection patterns comparing the mouse (Nelson et al., 2021) to our rat

findings. For example, we find a greater proportionate output of corticospinal projections to the thalamus, red nucleus and nucleus cuneatus in the rat than in the mouse, indicating potential differences in modulation of motor control.

In primates, previous work demonstrated that corticospinal axon terminals in the spinal cord are most dense in the intermediate gray matter (which contains dendrites of both spinal motoneurons and spinal interneurons), and some corticospinal axons extend into the motoneuron pools themselves (Kuypers, 1960; Liu and Chambers, 1964; Kuypers and Brinkman, 1970; Lawrence et al., 1985; Ralston and Ralston, 1985; Galea and Darian-Smith, 1994, 1997; Dum and Strick, 1996; Rosenzweig et al., 2009). Electrophysiological studies confirm the presence of direct corticomotoneuronal projections in macaques (Cooper, 1927; Preston and Whilock, 1960; Phillips and Porter, 1964; Fetz et al., 1976, 1980, Bernhard and Bohm, 1954; Jankowska et al., 1975; Cheney and Fetz, 1985; R. Porter, 1993; McKiernan et al., 1998; Nakajima et al., 2000; Lemon and Griffiths, 2005; Zaaimi et al., 2012; Morecraft et al., 2013). Findings of our study indicate that most of these corticospinal projections to lamina VII are likely synapsing on dendrites of alpha motoneurons that extend from the lateral motor neuron pools in intermediate spinal gray matter (Lawrence et al., 1985). We also find that approximately 20% of corticospinal projections to the spinal cord are synaptically connected to interneurons, including inhibitory interneurons, consistent with previous electrophysiological reports (Jankowska et al., 1976; Cheney and Fetz, 1985). We note the hypothetical possibility that anterograde trans-synaptic transport of either HSV or AAV1 might differ across synapses of different neuronal subclasses, thereby affecting the numerical frequency of post-synaptic targets identified in this study. The latter is a limitation intrinsic to any trans-synaptic tracing study.

How generalizable are the findings obtained here in rhesus macaques to other primate species, including humans? The corticospinal projection is lacking or minimally developed in some smaller primate species such as the marmoset and squirrel monkey, and these species lack the degree of fine dexterity of other primates such as rhesus macaques and humans, e.g., in prehensile actions such as thumb-index finger opposition precision grip. Humans and rhesus macaques share a command of fine motor dexterity, and it is likely that the anatomy identified in this study will mirror primates with similar motor capabilities, including humans. This highlights the relevance of rhesus macaque and cynomolgous primates as perhaps the most representative available model system to humans.

The contrasting nature of the corticospinal projection in rats versus primates has implications for understanding the consequences of injury to the CNS, and to human translation of candidate therapies to promote recovery of function after injury. Cortical injury results in far greater proportional loss of voluntary motor function in rhesus macaques than rodents: in mice and rats, complete ablation of the motor cortex spares non-skilled motor functions including locomotion and non-skilled forelimb use (Whishaw et al., 1991; Kawai et al., 2015; Gu et al., 2017; Lemon, 2019), whereas similar lesions in humans following stroke or traumatic brain injury can result in permanent and complete loss of *all* motor function (Laplane et al., 1977; Taub et al., 1993; Darling et al., 2009, 2011) other than spinal reflex movement. Thus the remarkable motor skills of primates come at a cost of devastating loss of function after injury to the brain. In contrast, redundant but less complex

motor output pathways in rodents (e.g., the rubrospinal projection) can compensate for the loss of primary motor cortex after injury. The macaque corticospinal projection exhibits a greater degree of spontaneous anatomical plasticity (sprouting) in the spinal cord after *partial* spinal cord injury than rodents (Rosenzweig et al., 2010; Friedli et al., 2015), and this is associated with spontaneous functional improvement in primates that exceeds that observed in rodents (Friedli et al., 2015). Thus, the primacy of corticospinal projections in macaque voluntary motor control suggests that strategies for promoting functional recovery in primates must include the corticospinal system. Brainstem projections to the spinal cord (e.g., reticulospinal) in primates also influence motor function, and we now find that these projections also receive direct corticospinal input. The most promising therapies for restoring motor function will consider all of these systems acting synergistically.

STAR ONLINE METHODS

Lead Contact

Further information and requests for resources and reagents should be directed to Mark Tuszynski (mtuszynski@health.ucsd.edu)

Material availability

This study did not generate any unique materials

Data and Code availability

This study did not use any unique analysis scripts

Experimental Model and Subject Details

Rat studies: For all rat studies adult Fischer 344 male rats were used (n= 4 for intersectional tracing studies and n=5 for HSV anterograde tracing studies). Animals were group housed (2 per cage) on a 12 h light/dark cycle with *ad libitum* access to food and water.

Primate studies: Adult rhesus macaques (Macaca mulatta, n=4 males for intersectional tracing studies and n=2 for AAV1 anterograde tracing studies, age 8–10 years) were subjects of this study. Subjects were housed and surgeries performed at the California National Primate Research Center; all primates procedures were approved by the California National Primate Research Center Institutional Animal Care and Use Committee. Subsequent tissue processing and analysis were performed at the Center for Neural Repair (University of California, San Diego (UCSD). For both rat and primate studies, all surgical and experimental procedures adhered to principles outlined by the American Association for the Accreditation of Laboratory Animal Care.

I. RAT METHODS

Intersectional Viral Tracing: To selectively induce Cre expression in corticospinal neurons associated with forelimb motor control (those projecting to spinal cord levels C7-T1), an intersectional viral approach was used. Adult rats were anesthetized and a laminectomy of the C6-C7 vertebral processes was performed. A Cre-encoding virus (AAV9-CAMKII-Cre-

SV40; Penn Vector Core) was injected at 3 sites per segment within the C7-T1 spinal segments (200 nl/injection) at 1100 and 700 μm below the dorsal spinal cord surface at each site (rate = 200 nl/min). In the same surgical session, a virus encoding a Cre-dependent membrane-targeted fluorescent tracer (AAVDJ-CAG-FLEX-ArchT-tdTomato; Salk Institute GT3 core) was injected into the right motor cortex; 200 nl virus was injected at a single depth (1000 μm below the cortical surface) at 10 evenly spaced sites within the forelimb area of the primary motor cortex (AP = −1.0 → +1.0; M/L = 2.5 → 4.25 relative to Bregma). Animals survived 4–5 weeks before being perfused.

For HSV anterograde trans-synaptic labeling, a Cre dependent HSV1 variant was used (HSV129ΔTK-TT) that has defects in retrograde trans-synaptic spread and is predominantly transported trans-synaptically in the anterograde direction (Lo and Anderson, 2011; Wojaczynski et al., 2015). To drive HSV129ΔTK-TT anterograde trans-synaptic spread specifically from C7-T1-projecting corticospinal neurons, the viral intersect approach was used. In an initial surgical session, the retrogradely targeted Cre virus was injected into the C7-T1 spinal segments as above. Following a 3-week interval, a Cre-dependent variant of the HSV-H129 virus (HSV-H129ΔTK-tdTomato; generous gift from Lynn Enquist, CNNV, Princeton) was injected into the forelimb cortex (150 nl) at the following coordinates:: A/P = 0.0; M/L = 3.25; D/V = 1.0). Animals were housed in a BSL-2 facility for 48–96 hours after delivering the HSV virus and were then harvested for analysis. A total of 8 animals were used for anterograde trans-synaptic tracing and 3 animals were eventually excluded due to no evidence of trans-synaptic spread.

We assessed anterograde trans-synaptic labelling in the spinal cords of rats using a second viral intersectional tool, the same tool that we subsequently used in rhesus monkeys: injections of AAV1-Cre into the motor cortex (AAV-1 undergoes *anterograde* trans-synaptic spread into spinal cord motoneurons), combined with Cre-dependent AAVDJ-FLEX-TdTomato injections in the spinal cord (N = 4 rats). The vector injected into the motor cortex expressed a destabilized Cre (Sando et al., 2013) to eliminate neuronal toxicity (pAAV-hSyn1-ddCre; 4 sites/hemisphere at 1.20mm from Bregma; 200ul/site), allowing Cre expression over 3 serial days in which trimethoprim (170 mg/kg) was intraperitoneally injected (Sando et al., 2013). In the spinal cord, Cre-dependent TdTomato (AAVDJ-FLEX-ArchT-TdTomato) was injected into six sites spanning C7-T1; injections were placed 0.5mm lateral to the spinal cord midline on the right side, at two depths of 0.5mm and 1mm form the dorsal spinal cord surface, at a volume of 500 nl/site.

Lastly, to demonstrate synaptic function in brain regions receiving collateral innervation by corticospinal axons, a viral intersect approach was used combining injection of Cre-dependent channel-rhodopsin (AAV8-FLEX-ChR2-GFP; UNC Vector Core) into the motor the cortex with injections of AAV-retro-Cre into spinal cord segments C7-T1 (N = 5 rats). Injections were placed into 4-week-old rats; the coordinates and injections described for AAVDJ-CAG-FLEX-ArchT-tdTomato injections were used.

Electrophysiology: Adult rats (P55 – 59) with channelrhodopsin-2 targeted specifically to C7-T1-projecting corticospinal neurons were anesthetized and perfused for 3 minutes with ice-cold, oxygenated, modified sucrose artificial cerebrospinal fluid (ACSF) containing

(in mM) 75 NaCl, 2.5 KCl, 3.3 MgSO4, 0.5 191 CaCl2, 1NaH2PO4, 26.2 NaHCO3, 22 glucose, 52.6 sucrose, 10 HEPES, 10 choline chloride, 1 pyruvate, 1 L-ascorbic acid (~300 mOsml, pH 7.4). The brain was rapidly dissected and 330 μm-thick slices containing regions of interest were cut on a vibratome (Leica VT1200). Slices were transferred to an opaque interface chamber containing the same modified sucrose ACSF solution and incubated at 34° C for 30 min then held at room temperature in the interface chamber for at least 45 min before initiating recordings. Recordings were made in a submersion-type recording chamber and perfused with oxygenated ACSF containing (in mM) 119 NaCl, 2.5 KCl, 2 MgCl2, 2.5 CaCl2, 1.3 NaH2PO4, 26.0 NaHCO3, 20 glucose (~295 mOsml) at 23° C at a rate of 2–3 ml / minute. Whole-cell patch clamp recordings were obtained using Multiclamp 700B patch amplifiers (Molecular Devices) and data were analyzed using pClamp 10 software (Molecular Devices). Data were low-pass filtered at 2 kHz, and digitized at 10 kHz. Whole-cell voltage and current clamp recordings were made at room temperature using pulled patch pipettes (5–6 MΩ) filled with internal solution containing (in mM) 150 K-Gluconate, 1.5 MgCl2, 5.0 HEPES, 1 EGTA, 10 phosphocreatine, 2.0 ATP, and 0.3 GTP. In all cases, the general health of the postsynaptic cell was confirmed by its ability to generate a series of action potential following current injection. Channelrhodopsin-2 positive terminals were activated by single pulses (5–50 msec duration; 25 sec interstimulus interval) of blue light (473 nm) delivered either through the microscope objective or via an external fiber optic cable (Thor Labs). In all cases, postsynaptic responses due to bulk photo-stimulation of corticospinal axons were evaluated over 5–30 sweeps in cells held at −65mV in voltage clamp. To isolate only monosynaptic responses in a subset of cells,1 μM TTX (Tocris Biosciences) and 250 μM 4-Aminopyridine (4-AP, Tocris Biosciences) was added to the bath.

Tissue processing: Animals were deeply anesthetized and transcardially perfused with 4% paraformaldehyde in 0.1M phosphate buffer. Brains and spinal cords were removed and post-fixed overnight before being transferred into 30% sucrose in 0.1M phosphate buffer for 2–3 days. The entire neuraxis from each subject was sectioned on a microtome set to 40 μm thickness and tissues were collected as a 1:12 transverse series in 0.1M phosphate buffer with 0.06% sodium azide. Nerve roots were used to identify spinal cord levels.

Immunohistochemistry: Sections were immunolabled for TdTomato as previously described (Adler et al., 2017) using a primary antibody against RFP (AbCam 73 34771; 1:5000 dilution) and secondary donkey anti-rabbit (Jackson Labs; 1: 500 dilution). Sections were then incubated sequentially with avidin-biotin complex (ABC kit; Vector Labs, 30 minutes) and with biotinyl tyramide (1:2500 dilution for 30 minutes), then incubated overnight with Alexa 594 conjugated streptavidin (1: 80 400 dilution; Jackson Labs). Sections were mounted onto glass slides and coverslipped with mowiol (http://cshprotocols.cshlp.org/content/2006/1/pdb.rec10255) mounting medium. A panel of antibodies was used to identify the polysynaptic targets of corticospinal projections in the spinal cord after trans-synaptic HSV administration, including: Ap2b for motor synergy encoder (MSE) neurons (Levine et al., 2014) (rabbit antibody from Santa Cruz Biotechnology; 1:200), Chx10 for motor interneurons (Briscoe et al., 2000; Ericson et al., 1997; sheep antibody from 92 Abcam; 1:200), ChAT for both alpha motoneurons and V0c neurons (Zagoraiou et al., 2009) (goat

antibody from Genetex; 1:200) and parvalbiumin (mouse antibody from Swant; 1:2000). A minimum of two sections per animal were labeled at each of spinal cord segments C2–4 and C7-T1.

Imaging: Imaging was performed using a Keyence BZ-X710 automated microscope and imaging system. Tiled images across individual brain slices were acquired using a 10X objective (1.4 NA) at a single focal plane (no Z-stack) using a Texas Red filter to detect TdTomato. Following imaging in the red channel, identically positioned image tiles were collected from the same brain slices using a GFP filter to detect autofluorescence. For each wavelength, the acquisition parameters were kept constant throughout the imaging process for all animals. All image tiles from individual brain slices were stitched using Keyence image analysis software and green and red images for each slice were processed using Adobe Photoshop. (For complete list of anatomical structures images see Supp. Table 1).

Axonal quantification: Raw images of brain and spinal cord sections were imported into FIJI (Schindelin et al., 2012) and the red channel was thresholded at a constant level across all sections for a given animal. Thresholded images were exported into Adobe Photoshop software and green images were superimposed to identify anatomical structures (Paxinos and Watson, 2013). Regions of interest (ROI) were drawn in each structure and corticospinal fiber density was measured in the red channel using the density analysis measurement option in FIJI, which yields a range of 0–255 based on pixel density within the ROI. Overall pixel measures for each ROI were computed by averaging values from at least 2 different sections in the same animal. For the spinal cord, ROIs associated with distinct laminae were identified within each segment according to previously described anatomical boundaries (M et al., 2013). For the brain and brainstem, volumes were calculated using a labeled 1:4 series of sections cut at 40 μm. For each brain slice, the ROI containing corticospinal projections was outlined and the axon density per unit area was multiplied by the section thickness (40 μm), and then axon volume measures for the structure were calculated by summing all sections for a given structure and multiplying by 4, the section sampling frequency. For the spinal cord, axon density per unit area of each ROI was multiplied by the length of the spinal segment (based upon the distance between nerve roots). The average segment length across cervical, thoracic, and lumbar segments was 2.61 ± 0.25 mm (mean ± SD). The proportional corticospinal input volume for a given structure was then calculated as axon volume within that structure divided by the total corticospinal axon volume of all structures receiving corticospinal innervation.

3D Reconstruction: Merged green and red images from a complete 1 in 4 series were registered and aligned in FIJI using a combination of “TurboReg” and “Align by Line ROI” registration plugins. TdTomato-labeled corticospinal cell bodies in motor cortex were imaged at lower fluorescence intensity than axons. Registered RGB TIFF image series were imported into Imaris (Bitplane Inc.) for 3D volumetric assembly and 3D surface rendering of the C7-T1-projecting corticospinal projection. A rendered volume of the labeled corticospinal projection was generated as a maximum intensity projection of the imported RGB image stack using the Imaris Surpass module. 3D isosurface rendering was performed on the red channel using the Surfaces function of the Imaris Surpass module.

Structures to be included in the surface rendering were selected using global thresholding and then filtered to remove non-specific background signal by subtraction of regions with volumes less than 5 μm^3. The number and distribution of retrogradely labeled corticospinal cell bodies was obtained from the blue channel using the Spots function of the 180 Imaris surpass module. Movies were generated using the Imaris Animation module and exported as ".mov" files. Annotations were added using iMovie (Apple Inc.). Individual images showing intensity heat maps for the 3D rendered C-8 corticospinal projection were generated in FIJI using the 3D projection function and a custom look up table (LUT) ranging from 0–255 derived from the same color scale used to generate the heat maps described previously (Blue= 186 0.0, yellow= median, red= 246)

II. PRIMATE METHODS

Intersectional Viral Tracing, Primate Studies: As in rat studies, we used a viral intersectional approach to selectively induce Cre expression in corticospinal neurons associated with forelimb fine motor control in rhesus macaques. Study subjects (n=4) were anesthetized and the C7-T1 spinal cord levels were exposed. 30-ga injection pipettes (Molex) filled with AAVrg-pmSyn1-EBFP-Cre (2×10^{12} vg/ml) were injected into 10 sites of the right spinal cord. Injection sites were 1.5 mm apart in the rostro-caudal axis and 0.7 mm medial to the medial aspect of the dorsal root entry zone. Two injection depths per site [2.5 mm, 3.5 mm] each received 1.25 µl of vector at a rate of 0.5 µl/min. In the same surgical session, a craniotomy was performed and Cre-dependent membrane-targeted fluorescent tracer (AAVdj-CAG-DIO-gCOMET, Salk Institute GT3 core, 1.2×10^{12} genome copies / ml) was injected into the left primary motor cortex. Injections were made at 28 evenly spaced sites within the area controlling forelimb function at a mediolateral range of 13.3 to 24.5 mm lateral to midline. 14 sites were located 1.5 mm rostral to the central sulcus, and 14 sites were 2.5 mm rostral to the central sulcus (Rosenzweig et al., 2010). 300 nl of vector were injected per site using fine-tipped pulled glass micropipettes at depths of 2, 3.5, and 5.5 mm from the cortical surface, for a total of 84 injections. Subjects were euthanized 3 months later.

To determine anterograde trans-synaptic partners of corticospinal axons in the macaque spinal cord (n=2), we used methods described for rat studies above. pAAV-hSyn1-ddCre (expressing destabilized Cre) was injected into 84 sites of the left primary motor cortex at coordinates listed in preceding paragraph; we subsequently activated Cre expression for 3 serial days using intraperitoneal injections of Trimethoprim (170 mg/kg) (Sando et al., 2013); Trimethoprim was later administered as described below to transiently activate Cre expression and anterograde transport. During the same surgical initial session, Cre dependent AVVDJ-FLEX-ArchT-TdTomato was injected into 10 sites per side of the spinal cord: injections were placed 2 mm lateral to the spinal cord midline bilaterally, and at 1.5mm rostral-to-caudal intervals spanning C7-T1. Each site was injected at 3 depths located 2, 3 and 4 mm ventral to the dorsal spinal cord surface, at a volume of 1.7ul/depth. Trimethoprim (TMP) was administered subcutaneously for 3 days (170mg/kg) starting one month after vector injections. A mean of 2185 ± 207 layer V corticospinal neurons were labelled among these 4 monkeys.

Tissue processing: Subjects were very deeply anesthetized and transcardially perfused with 4% PFA. Brains and spinal cords were sectioned in the transverse plane throughout the neuraxis. Tissue was cut on a microtome set at 40 μm thickness and sections were stored at −20 °C in cryoprotectant.

Immunohistochemistry: Sections were immunolabled for gCOMET as described previously (Rosenzweig et al., 2018) by overnight incubation at 4°C in the following primary antibody solution against: anti-GFP (to label all corticospinal axon collaterals; Aves chicken Ab at 1:2000 dilution), anti-RFP (contralateral corticospinal axon collaterals; Rockland rabbit Ab at 1:2000 dilution), anti-NeuN (to label neurons; Encor mouse Ab at 1:2000 dilution), anti-ChAT (to label spinal motoneurons; Genetex goat Ab at 1:250 dilution), anti-parvalbiumin (mouse antibody from Swant; 1:2000), anti-synaptophysin (to identify pre-synaptic terminals; Chemicon mouse Ab at 1:1000 dilution), anti-Satb1 (to identify motor synergy encoder neurons; Santa biotechnology goat antibody at 1:1000 dilution). Sections were then incubated with a secondary antibody solution containing anti-chicken 488 (Life Tech 703-545-155; 1: 500 dilution), anti- rabbit 567 (Life Tech A10042; 1: 500 dilution), and anti-mouse 647 (Life Tech 31571; 1: 500 dilution), followed by DAPI nuclear stain (Sigma D-9542, 1:1,000). Sections were coverslipped with mowiol (http://cshprotocols.cshlp.org/content/2006/1/pdb.rec10255).

Imaging: For imaging of corticospinal axon terminals throughout the neuraxis, we used methods described for rat studies. Briefly, a GFP filter detected gCOMET and a TriTC red filter detected background tissue architecture due to autofluorescence (Fig 4D shows the section post background removal). For brain structures, 10x tiled images were acquired to locate structures receiving corticospinal innervation, and these regions of interest were then acquired at 200X magnification. For spinal cord sections, the entire section was imaged at 200X. For each wavelength, the acquisition parameters were kept constant throughout the imaging process for all animals. All image tiles from individual brain slices were stitched using Keyence image analysis software. (For complete list of anatomical structures images see Supp. Table 1).

Axonal quantification: We used methods similar to those described for rats. Acquired red-green-blue images were imported into Adobe Photoshop. Non-specific background was removed by eliminating the blue and yellow channels. The green image was imported into FIJI (Schindelin et al., 2012) and our automated script converted each image into 8-bits that were thresholded (using constant values applied to images from to yield axon length in pixels per unit area. Nissl stained sections were compared to brainmaps (http://brainmaps.org/index.php) to identify brain structures. Axon densities in each section from a given structure were summed and multiplied by the section sampling frequency (brain 1:24; spinal cord 1:48) leading to a total axon density measure per structure. As in rats, the proportional corticospinal input volume for a given structure was then calculated as axon volume within that structure divided by the total corticospinal axon volume of all structures receiving corticospinal innervation.

Supplementary Material

Refer to Web version on PubMed Central for supplementary material.

ACKNOWLEDGMENTS

We are grateful for expert technical assistance of Amanda Tran, Terri Grider, Christopher Mannion, John Hyde, Rachele Wurr, Ryan Macon, and Stephanie Hawbecker.

Funding:

This work was supported by the National Institutes of Health (NS042291 to MHT; NS 105478 to JCB/MSB/MHT), the Veterans Administration Gordon Mansfield Consortium (IP50RX001045 and RR&D B7332R to MHT and 1I01RX002245 to ARF), the Craig H. Neilsen Foundation, the Bernard and Anne Spitzer Charitable Trust, Dr. Miriam and Sheldon G. Adelson Medical Research Foundation (MHT/LAH), and the Gerbic Family Foundation. The California National Primate Research Center is funded by NCRR P51 OD011107-56.

BIBLIOGRAPHY

Abraira VE, Ginty DD (2013) The sensory neurons of touch. Neuron 79:618–639. [PubMed: 23972592]

Adams RA, Shipp S, Friston KJ (2013) Predictions not commands: Active inference in the motor system. Brain Struct Funct 218:611–643. [PubMed: 23129312]

Adler AF, Lee-Kubli C, Kumamaru H, Kadoya K, Tuszynski MH (2017) Comprehensive Monosynaptic Rabies Virus Mapping of Host Connectivity with Neural Progenitor Grafts after Spinal Cord Injury. Stem Cell Reports 8:1525–1533. [PubMed: 28479302]

Akintunde A, Buxton DF (1992) Differential sites of origin and collateralization of corticospinal neurons in the rat: a multiple fluorescent retrograde tracer study. Brain Res 575:86–92. [PubMed: 1504786]

Alstermark B, Isa T (2012) Circuits for Skilled Reaching and Grasping. Annu Rev Neurosci 35:559–578. [PubMed: 22524789]

Azim E, Alstermark B (2015) Skilled forelimb movements and internal copy motor circuits. Curr Opin Neurobiol 33:16–24. [PubMed: 25588912]

Azim E, Jiang J, Alstermark B, Jessell TM (2014) Skilled reaching relies on a V2a propriospinal internal copy circuit. Nature 508:357–363. [PubMed: 24487617]

Bernhard CG, Bohm E (1954) Cortical representation and functional significance of the corticomotoneuronal system. Arch Neurol Psychiatry 72:473–502. [PubMed: 13206470]

Biane JS, Takashima Y, Scanziani M, Conner JM, Tuszynski MH (2016) Thalamocortical Projections onto Behaviorally Relevant Neurons Exhibit Plasticity during Adult Motor Learning. Neuron 89:1173–1179. [PubMed: 26948893]

Biane JS, Takashima Y, Scanziani M, Conner JM, Tuszynski MH (2019) Reorganization of recurrent layer 5 corticospinal networks following adult motor training. J Neurosci 39:4684–4693. [PubMed: 30948479]

Blakemore SJ, Wolpert D, Frith C (2000) Why can't you tickle yourself? Neuroreport 11:R11–R16. [PubMed: 10943682]

Bortoff GA, Strick PL (1993) Corticospinal terminations in two new-world primates: Further evidence that corticomotoneuronal connections provide part of the neural substrate for manual dexterity. J Neurosci 13:5105–5118. [PubMed: 7504721]

Briscoe J, Pierani A, Jessell TM, Ericson J (2000) A homeodomain protein code specifies progenitor cell identity and neuronal fate in the ventral neural tube. Cell 101:435–445. [PubMed: 10830170]

Canedo A (1997) Primary motor cortex influences on the descending and ascending systems. Prog Neurobiol 51:287–335. [PubMed: 9089791]

Cheney PD, Fetz EE (1985) Comparable patterns of muscle facilitation evoked by individual corticomotoneuronal (CM) cells and by single intracortical microstimuli in primates: Evidence for functional groups of CM cells. J Neurophysiol 53:786–804. [PubMed: 2984354]

Cook-Snyder DR, Jones A, Reijmers LG (2015) A retrograde adeno-associated virus for collecting ribosome-bound mRNA from anatomically defined projection neurons. Front Mol Neurosci 8: article 56. [PubMed: 26557053]

Cooper S (1927) Responses to stimulation of the motor area of the cerebral cortex. Proc R Soc London Ser B, Contain Pap a Biol Character 102:222–236.

Crapse TB, Sommer MA (2008) Corollary discharge across the animal kingdom. Nat Rev Neurosci 9:587–600. [PubMed: 18641666]

Cruikshank SJ, Urabe H, Nurmikko AV, Connors BW (2010) Pathway-Specific Feedforward Circuits between Thalamus and Neocortex Revealed by Selective Optical Stimulation of Axons. Neuron 65:230–245. [PubMed: 20152129]

Cullen KE (2004) Sensory signals during active versus passive movement. Curr Opin Neurobiol 14:698–706. [PubMed: 15582371]

Darling WG, Pizzimenti MA, Morecraft RJ (2011) Functional Recovery Following Motor Cortex Lesions In Non-Human Primates: Experimental Implications For Human Stroke Patients. J Integr Neurosci 10:353–384. [PubMed: 21960307]

Darling WG, Pizzimenti MA, Rotella DL, Peterson CR, Hynes SM, Ge J, Solon K, McNeal DW, Stilwell-Morecraft KS, Morecraft RJ (2009) Volumetric effects of motor cortex injury on recovery of dexterous movements. Exp Neurol 220:90–108. [PubMed: 19679127]

Deschênes M, Bourassa J, Pinault D (1994) Corticothalamic projections from layer V cells in rat are collaterals of long-range corticofugal axons. Brain Res 664:215–219. [PubMed: 7895031]

Dum RP, Strick PL (1996) Spinal cord terminations of the medial wall motor areas in macaque monkeys. J Neurosci 16:6513–6525. [PubMed: 8815929]

Elmallah MK, Falk DJ, Lane MA, Conlon TJ, Lee KZ, Shafi NI, Reier PJ, Byrne BJ, Fuller DD (2012) Retrograde gene delivery to hypoglossal motoneurons using adeno-associated virus serotype 9. Hum Gene Ther Methods 23:148–156. [PubMed: 22693957]

Ericson J, Rashbass P, Schedl A, Brenner-Morton S, Kawakami A, Van Heyningen V, Jessell TM, Briscoe J (1997) Pax6 controls progenitor cell identity and neuronal fate in response to graded Shh signaling. Cell 90:169–180. [PubMed: 9230312]

Fetz EE, Cheney PD (1980) Postspike facilitation of forelimb muscle activity by primate corticomotoneuronal cells. J Neurophysiol 44:751–772. [PubMed: 6253604]

Fetz EE, Cheney PD, German DC (1976) Corticomotoneuronal connections of precentral cells detected by post-spike averages of EMG activity in behaving monkeys. Brain Res 114:505–510. [PubMed: 821592]

Friedli L, Rosenzweig ES, Barraud Q, Schubert M, Dominici N, Awai L, Nielson JL, Musienko P, Nout-Lomas Y, Zhong H, Zdunowski S, Roy RR, Strand SC, Van Den Brand R, Havton LA, Beattie MS, Bresnahan JC, Bézard E, Bloch J,Edgerton VR,Ferguson AR Curt A, Tuszynski MH,Courtine G (2015) Pronounced species divergence in corticospinal tract reorganization and functional recovery after lateralized spinal cord injury favors primates. Sci Transl Med 7:302

Galea MP, Darian-Smith I (1994) Multiple corticospinal neuron populations in the macaque monkey are specified by their unique cortical origins, spinal terminations, and connections. Cereb Cortex 4:166–194. [PubMed: 8038567]

Galea MP, Darian-Smith I (1997) Corticospinal projection patterns following unilateral section of the cervical spinal cord in the newborn and juvenile macaque monkey. J Comp Neurol 381:282–306. [PubMed: 9133569]

Georgopoulos AP, Carpenter AF (2015) Coding of movements in the motor cortex. Curr Opin Neurobiol 33:34–39. [PubMed: 25646932]

Green F, Samaranch L, Zhang HS, Manning-Bog A, Meyer K, Forsayeth J, Bankiewicz KS (2016) Axonal transport of AAV9 in nonhuman primate brain. Gene Ther 23:520–526. [PubMed: 26953486]

Hattox AM, Nelson SB (2007) Layer V neurons in mouse cortex projecting to different targets have distinct physiological properties. J Neurophysiol 98:3330–3340. [PubMed: 17898147]

Hoff EC, Hoff HE (1934) Spinal terminations of the projection fibres from the motor cortex of primates. Brain 57:454–474.

Huang LYM (1989) Origin of thalamically projecting somatosensory relay neurons in the immature rat. Brain Res 495:108–114. [PubMed: 2776029]

Jankowska E, Padel Y, Tanaka R (1975) Projections of pyramidal tract cells to alpha-motoneurones innervating hind-limb muscles in the monkey. J Physiol 249:637–667. [PubMed: 1177109]

Jankowska E, Padel Y, Tanakat R (1976) Disynaptic inhibition of spinal motoneurones from the motor cortex in the monkey. J Physiol 258:467–487. [PubMed: 822152]

Kalaska JF (2009) From intention to action: Motor cortex and the control of reaching movements. Adv Exp Med Biol 629:139–178. [PubMed: 19227499]

Kita T, Kita H (2012) The Subthalamic Nucleus Is One of Multiple Innervation Sites for Long-Range Corticofugal Axons: A Single-Axon Tracing Study in the Rat. J Neurosci 32:5990–5999. [PubMed: 22539859]

Kuypers HGJM(1960) Central cortical projections to motor and somato-sensory cell groups: An experimental study in the rhesus monkey. Brain 83:161–184. [PubMed: 14413010]

Kuypers HGJM, Brinkman J (1970) Precentral projections to different parts of the spinal intermediate zone in the rhesus monkey. Brain Res 24:29–48. [PubMed: 4099987]

Lacroix S, Havton LA, McKay H, Yang H, Brant A, Roberts J, Tuszynski MH (2004) Bilateral corticospinal projections arise from each motor cortex in the macaque monkey: a quantitative study. J Comp Neurol 473:147–161. [PubMed: 15101086]

Laplane D, Talairach J, Meininger V, Bancaud J, Bouchareine A (1977) Motor consequences of motor area ablations in man. J Neurol Sci 31:29–49. [PubMed: 833609]

Lawrence DG, Porter R, Redman SJ (1985) Corticomotoneuronal synapses in the monkey: Light microscopic localization upon motoneurons of intrinsic muscles of the hand. J Comp Neurol 232:499–510. [PubMed: 3980765]

Lemieux M, Id FB (2019) Glutamatergic neurons of the gigantocellular reticular nucleus shape locomotor pattern and rhythm in the freely behaving mouse. PLoS Biology 17:4

Lemon R (2019) Recent advances in our understanding of the primate corticospinal system. F1000 research 8:274

Lemon RN (2008) Descending Pathways in Motor Control. Annu Rev Neurosci 31:195–218. [PubMed: 18558853]

Lemon RN, Griffiths J (2005) Comparing the function of the corticospinal system in different species: Organizational differences for motor specialization? Muscle and Nerve 32:261–279. [PubMed: 15806550]

Leonelli S (2012) When humans are the exception: Cross-species databases at the interface of biological and clinical research. Soc Stud Sci 42:214–236. [PubMed: 22848998]

Lévesque M, Charara A, Gagnon S, Parent A, Deschênes M (1996) Corticostriatal projections from layer V cells in rat are collaterals of long-range corticofugal axons. Brain Res 709:311–315. [PubMed: 8833768]

Levine AJ, Hinckley CA, Hilde KL, Driscoll SP, Poon TH, Montgomery JM, Pfaff SL, Neurosci N (2014) Identification of a cellular node for motor control pathways. Nat Neurosci 17:586–593. [PubMed: 24609464]

Liu CN, Chambers WW (1964) An Experimental study of the cortico-spinal system in the monkey (Macaca mulatta). The spinal pathways and preterminal distribution of degenerating fibers following discrete lesions of the pre- and postcentral gyri and bulbar pyramid. J Comp Neurol 123:257–283. [PubMed: 14219668]

Lo L, Anderson DJ (2011) A cre-dependent, anterograde transsynaptic viral tracer for mapping output pathways of genetically marked neurons. Neuron 72:938–950. [PubMed: 22196330]

Harrison M, O'Brien A, Adams L, Cowin G, Ruitenberg MJ, Sengul G, Watson C (2013) Vertebral landmarks for the identification of spinal cord segments in the mouse. Neuroimage 68:22–29. [PubMed: 23246856]

Masamizu Y, Okada T, Kawasaki K, Ishibashi H, Yuasa S, Takeda S, Hasegawa I, Nakahara K (2011) Local and retrograde gene transfer into primate neuronal pathways via adeno-associated virus serotype 8 and 9. Neuroscience 193:249–258. [PubMed: 21782903]

McKiernan BJ, Marcario JK, Karrer JH, Cheney PD (1998) Corticomotoneuronal postspike effects in shoulder, elbow, wrist, digit, and intrinsic hand muscles during a reach and prehension task. J Neurophysiol 80:1961–1980. [PubMed: 9772253]

Miall RC, Wolpert DM (1996) Forward models for physiological motor control. Neural Networks 9:1265–1279. [PubMed: 12662535]

Morecraft RJ, Ge J, Stilwell-Morecraft KS, Mcneal DW, Pizzimenti MA, Darling WG (2013) Terminal distribution of the corticospinal projection from the hand/arm region of the primary motor cortex to the cervical enlargement in rhesus monkey. J Comp Neurol 521:4205–4235. [PubMed: 23840034]

Nakajima K, Maier MA, Kirkwood PA, Lemon RN (2000) Striking differences in transmission of corticospinal excitation to upper limb motoneurons in two primate species. J Neurophysiol 84:698–709. [PubMed: 10938297]

Nelson A, Abdelmesih B, Costa RM (2021) Corticospinal populations broadcast complex motor signals to coordinated spinal and striatal circuits. Nat Neurosci 24.

Parent M, Parent A (2006) Single-axon tracing study of corticostriatal projections arising from primary motor cortex in primates. J Comp Neurol 496:202–213. [PubMed: 16538675]

Paxinos G, Watson C (2013) The Rat Brain in Stereotaxic Coordinates. Elsevier Science.

Petreanu L, Huber D, Sobczyk A, Svoboda K (2007) Channelrhodopsin-2-assisted circuit mapping of long-range callosal projections. Nat Neurosci 10:663–668. [PubMed: 17435752]

Petreanu L, Mao T, Sternson SM, Svoboda K (2009) The subcellular organization of neocortical excitatory connections. Nature 457:1142–1145. [PubMed: 19151697]

Phillips CG, Porter R (1964) The Pyramidal Projection to Motoneurones of Some Muscle Groups of the Baboon's Forelimb. Prog Brain Res 12:222–245. [PubMed: 14202441]

Phillips CG, Porter R (1977) Corticospinal neurones. Their role in movement. Monogr Physiol Soc.

Preston JB, Whitlock DG (1960) Precentral facilitation and inhibition of spinal motoneurons. J Neurophysiol 23:154–170. [PubMed: 14434790]

Porter R, Lemon R (1993) Corticospinal function and voluntary movement. Monogrqaphs of the physiological society. Oxford Science Publications 45.

Ralston DD, Ralston HJ (1985) The terminations of corticospinal tract axons in the macaque monkey. J Comp Neurol 242:325–337. [PubMed: 2418074]

Rosenzweig ES, Brock JH, Culbertson MD, Lu P, Moseanko R, Edgerton VR, Havton LA, Tuszynski MH (2009) Extensive spinal decussation and bilateral termination of cervical corticospinal projections in rhesus monkeys. J Comp Neurol 513:151–163. [PubMed: 19125408]

Rosenzweig ES, Brock JH, Lu P, Kumamaru H, Salegio EA, Kadoya K, Weber JL, Liang JJ, Moseanko R, Hawbecker S, Huie JR, Havton LA, Nout-Lomas YS, Ferguson AR, Beattie MS, Bresnahan JC, Tuszynski MH (2018) Restorative effects of human neural stem cell grafts on the primate spinal cord. Nat Med 24:484–490. [PubMed: 29480894]

Rosenzweig ES, Courtine G, Jindrich DL, Brock JH, Ferguson AR, Strand SC, Nout YS, Roy RR, Miller DM, Beattie MS, Havton LA, Bresnahan JC, Edgerton VR, Tuszynski MH (2010) Extensive spontaneous plasticity of corticospinal projections after primate spinal cord injury. Nat Neurosci 13:1505–1510. [PubMed: 21076427]

Sando R, Baumgaertel K, Pieraut S, Torabi-Rander N, Wandless TJ, Mayford M, Maximov A (2013) Inducible control of gene expression with destabilized Cre. Nat Methods 10:1085–1091. [PubMed: 24056874]

Schindelin J, Arganda-Carreras I, Frise E, Kaynig V, Longair M, Pietzsch T, Preibisch S, Rueden C, Saalfeld S, Schmid B, Tinevez JY, White DJ, Hartenstein V, Eliceiri K, Tomancak P, Cardona A (2012) Fiji: An open-source platform for biological-image analysis. Nat Methods 9:676–682. [PubMed: 22743772]

Schwarz LA, Miyamichi K, Gao XJ, Beier KT, Weissbourd B, Deloach KE, Ren J, Ibanes S, Malenka RC, Kremer EJ, Luo L (2015) Viral-genetic tracing of the input-output organization of a central noradrenaline circuit. Nature 524:88–92. [PubMed: 26131933]

Scott SH (2004) Optimal feedback control and the neural basis of volitional motor control. Nat Rev Neurosci 5:532–544. [PubMed: 15208695]

Shadmehr R, Smith MA, Krakauer JW (2010) Error correction, sensory prediction, and adaptation in motor control. Annu Rev Neurosci 33:89–108. [PubMed: 20367317]

Taub E, Miller NE, Novack TA, Cook EW, Fleming WC, Nepomuceno CS, Connell JS, Crago JE (1993) Technique to improve chronic motor deficit after stroke. Arch Phys Med Rehabil 74:347–354. [PubMed: 8466415]

Wojaczynski GJ, Engel EA, Steren KE, Enquist LW, Patrick Card J (2015) The neuroinvasive profiles of H129 (herpes simplex virus type 1) recombinants with putative anterograde-only transneuronal spread properties. Brain Struct Funct 220:1395–1420. [PubMed: 24585022]

Zaaimi B, Edgley SA, Soteropoulos DS, Baker SN (2012) Changes in descending motor pathway connectivity after corticospinal tract lesion in macaque monkey. Brain 135:2277–2289. [PubMed: 22581799]

Zagoraiou L, Akay T, Martin JF, Brownstone RM, Jessell TM, Miles GB (2009) A Cluster of Cholinergic Premotor Interneurons Modulates Mouse Locomotor Activity. Neuron 64:645–662. [PubMed: 20005822]

Zingg B, Chou X lin, Zhang Z gang, Mesik L, Liang F, Tao HW, Zhang LI (2017) AAV-Mediated Anterograde Transsynaptic Tagging: Mapping Corticocollicular Input-Defined Neural Pathways for Defense Behaviors. Neuron 93:33–47. [PubMed: 27989459]

Highlights

- The entire projectome of the corticospinal motor system is mapped in rats and monkeys
- The rat system elaborately collateralizes and integrates sensorimotor systems
- The primate system is far more restricted in accessing direct motor execution
- These differences between species have important implications for translational research

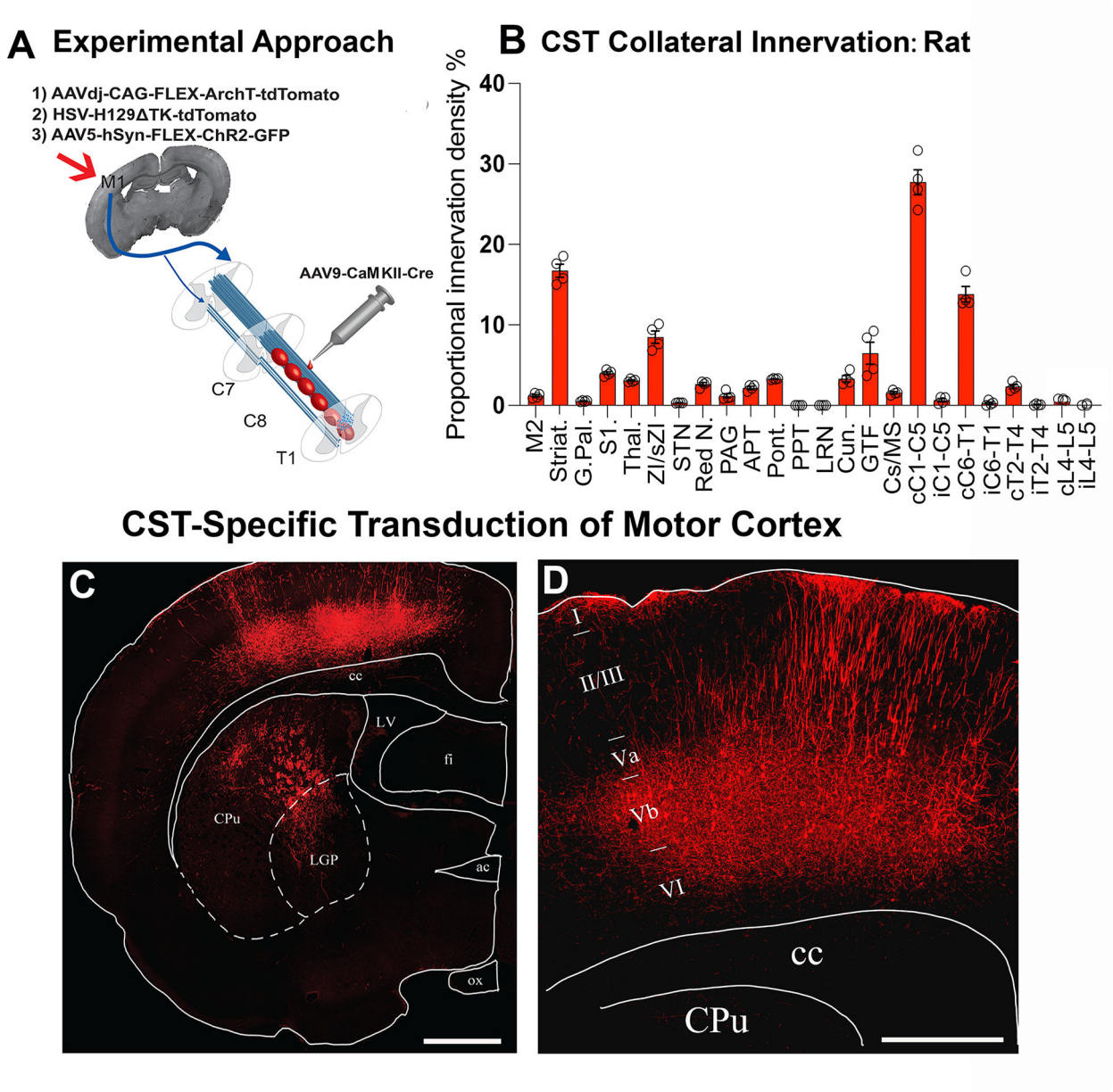

Figure 1: Experimental Design and Distribution of Corticospinal Collaterals in the Rat

(**A**) Experimental design and vectors used for forelimb targeted intersectional mapping of the corticospinal neuron. Cre-encoding AAV9-CAMKII-Cre-SV40 was injected in the forelimb controlling region of the spinal cord (C7-T1) and was retrogradely transported to the motor cortex, where Cre activated either: 1) AAVDJ-CAG-FLEX-ArchT-tdTomato, to map all corticspinal axon collaterals throughout the nervous system, 2) HSV-H129ΔTK-tdTomato, to anterogradely trace the mono- and polysynaptic targets of corticospinal axons projecting to distal forelimb-controlling regions of the cervical spinal cord, or 3) AAV8-FLEX-ChR2-GFP, to examine synaptic activity of corticospinal collaterals in various brain regions. (**B**) To quantify the innervation of the CST projectome per anatomical structure, axonal length in each target region was quantified and converted to a percentage of

total CST length in every anatomical structure from that animal. Total distribution of all corticospinal innervation in the rat neuraxis revealed only 13.8% of overall corticospinal axonal output (arising from C7-T1-projecting cortical neurons) terminates in the C6-T1 spinal cord and the majority terminates in *upper* cervical segments (C1-C5). The remainder of corticospinal axonal output associated with distal forelimb control terminates in several other structures in the brain. (**C**) Rat coronal brain section showing potency of retrograde Cre-dependent expression of tdTomato in layer 5 cortical neurons, and collateral innervation to caudate/putamen (CPut) and lateral globus pallidus (LGP). (**D**) Higher magnification view in M1 motor cortex showing transduction specifity to L5. Abbreviations: M1, Primary motor cortex; M2, sensorimotor cortex; Striat, striatum; G. Pal., globus pallidus; Thal, thalamus; ZI/SZI, zona incerta/subIncerta; STN, subthalamic n.; PAG, periaquadactal grey; APT, anterior pretectal n.; Pont., pontine n.; PPT, pedunculopontine tegmental n.; LRN, lateral reticular n.; Cun, cuneatus n.; GFT, gigantocellular tegmental field ; Cs/MS, superior colliculus/ mesencephalic nucleus; c, contralateral; i, ipsilateral. Scale bars: B,1.2mm; C, 200μm

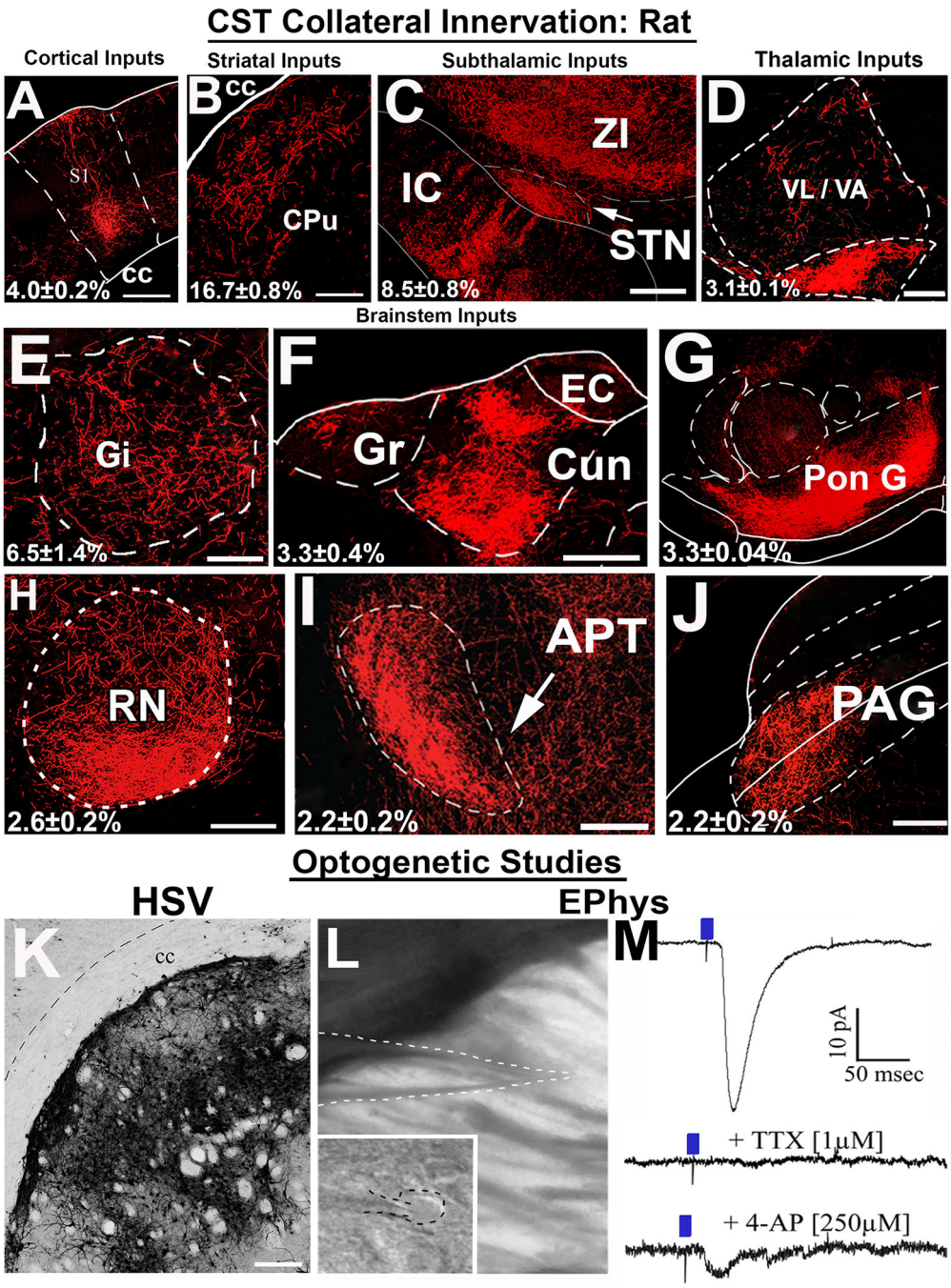

Figure 2: Examples of Distal Forelimb-Controlling Corticospinal Axon Collateral Projections to Brain Regions in the Rat

Corticospinal axon collateral terminals revealed by AAVDJ -FLEX-ArchT-TdTomato in (**A**) S1, primary sensory cortex, (**B**) caudate/putamen (CPu), (**C**) zona incerta (ZI), and subthalamic nucleus (STN;. IC, Internal Capsule), (**D**) VL/VA, ventrolateral ventroanterior thalamic nuclei, (**E**) Gi, gigantocellular tegmental field (**F**) cuneate nucleus (Cun), Gr, gracile nucleus and external cuneate nucleus (EC), **(G)** pontine gray (Pon G), **(H)** red nucleus. **(I)** anterior pretectal nucleus (APT), a sensory processing area, and **(J)** periaquactal

grey. (**K**) Anterograde HSV labeling shows the presence of post-synaptic neuronal targets of cortiospinal innervation to the caudate/putamen. (**L**) Optogenetic recordings in striatal slices after delivery of intersectional AAV8-FLEX-ChR2-GFP to the motor cortex; image shows location of recording pipette, and inset shows patching of a single cell. (**M**) With photoactivation using a 10ms laser pulse, excitatory post-synaptic currents are evoked. Application of tetrodotoxin (TTX) abolishes responses, and the K^+ channel blocker 4-aminopyridine (4-AP) partially restores responses, indicating the presence of direct, monosynaptic excitatory corticospinal projections in the striatum. Scale bars: A-J; 150μm, L; 100μm

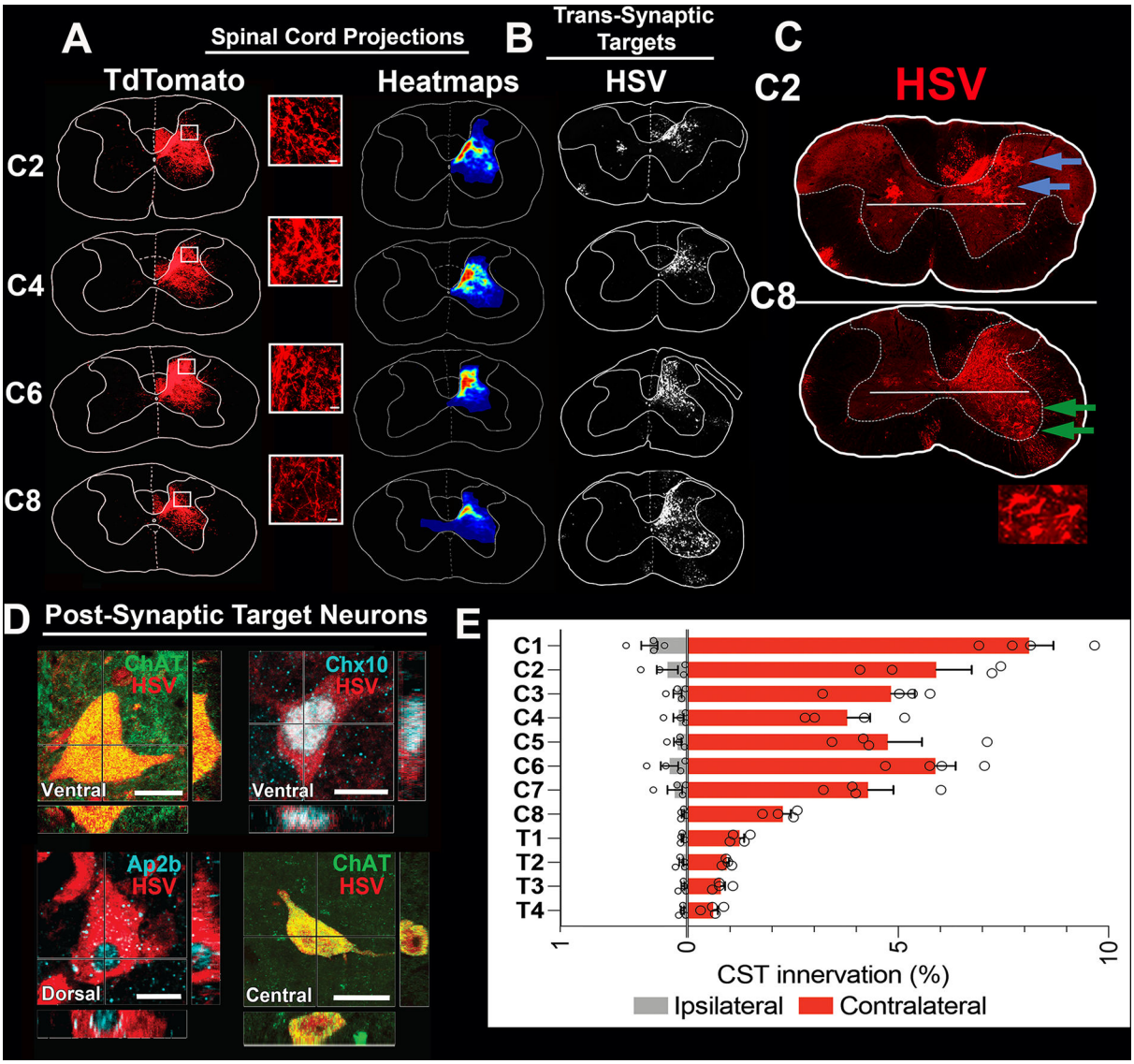

Figure 3: Corticospinal Projections and Poly-Synaptic Targets in the Rat Spinal Cord

(**A**) Corticospinal terminal zones throughout the cervical spinal cord after intersectional mapping initiated from forelimb-controlling spinal segments C7-T1. Despite initiation of mapping from forelimb-controlling segments C7-T1, there are greater numbers of corticospinal axon collaterals in upper than lower spinal cord segments (quantified in E). tdTomato images shown on left and heatmaps on right. (**B,C**) Spinal cord mono- and poly-synaptic targets were identified using intersectional anterograde trans-synaptic HSV. Notably, corticospinal projections in upper cervical segments predominantly target dorsal gray matter circuitry which is restricted to sensory neuronal regions (blue arrows); in contrast, lower cervical collaterals of the same axons access polysynaptic circuits that reach alpha motoneurons controlling the distal forelimb (green arrows). (**D**) Co-localization of poly-trans-synaptic HSV with cell type-specific markers reveals that corticospinal axons in lower cervical spinal cord segments project onto Ap2b motor synergy encoder neurons, Chx10-expressing V2a interneurons, and ChAT-expressing V0c motor interneurons as well

as ChAT-expressing alpha motoneurons., (**E**) Quantification of the proportional collateral innervation in the spinal segments C1-T4. Innervation ipsilateral to cortical injections on the left (grey), and contralateral to cortical injections in the right (red). Quantification showed increased innervation in upper cervical segements (C1-C5) Scale bars: D, 20μm.

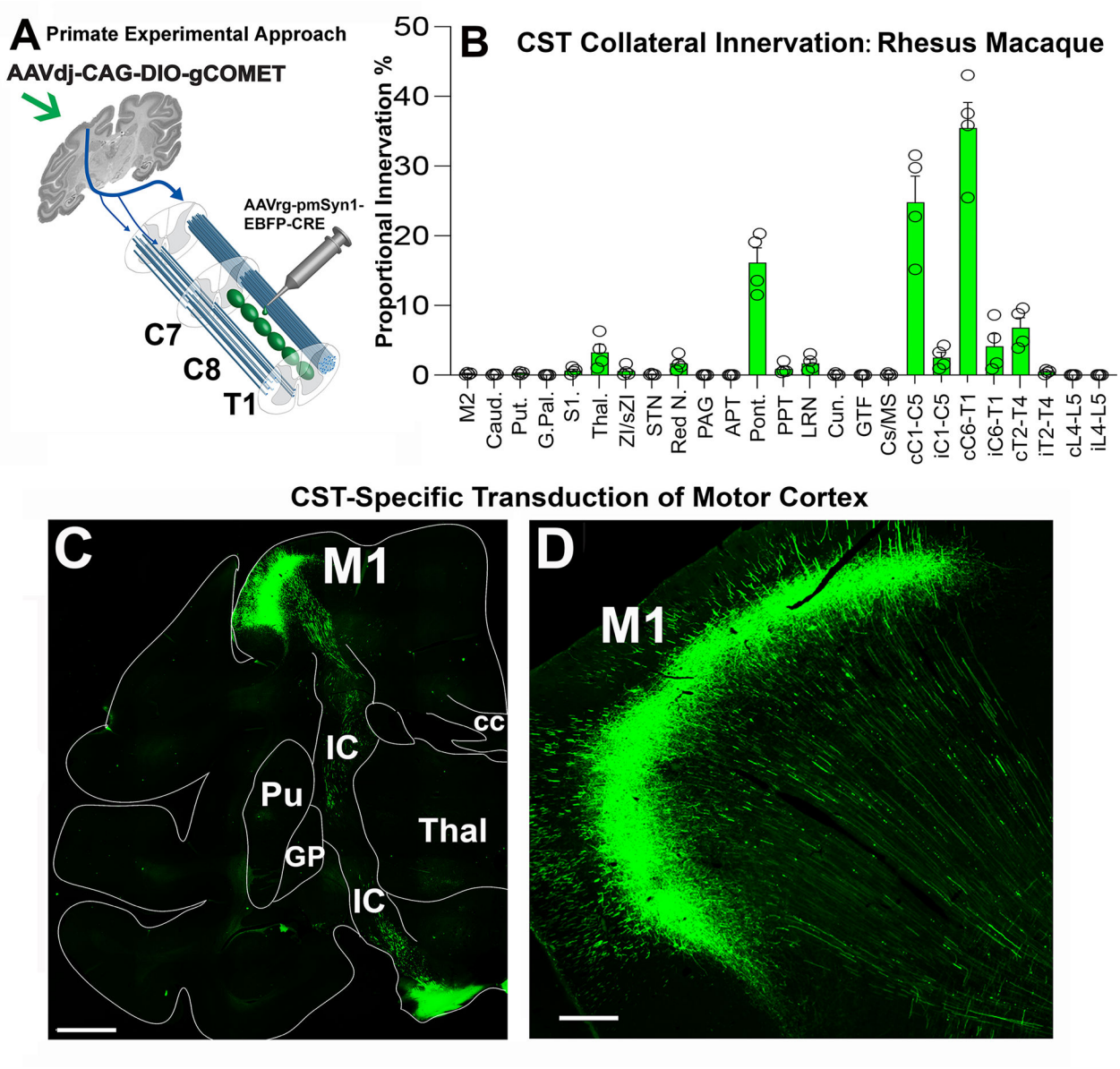

Figure 4: Experimental Design and Distribution of Corticospinal Collaterals in the Macaque

(**A**) Experimental design for forelimb targeted intersectional mapping of the corticospinal neuron. Cre-encoding AAVrg-pmSyn1-EBFP-Cre was injected in the forelimb area of the spinal cord (C7-T1) and Cre-dependent AAVdj-CAG-DIO-gCOMET tracer that was injected in layer V primary motor cortex. This allowed specific filling of all axonal processes arising from corticospinal neurons that control the hand. (**B**) Distribution of all corticospinal projections in the macaque neuraxis; the vast majority of projections terminate in the spinal cord, and particularly the contralateral lower cervical spinal cord (C6-T1). (**C**) Coronal section showing intersectional-targeted M1 corticospinal neurons and their projections in the brain. IC; internal capsule; Pu, putamen; GP, globus pallidus; Thal, thalamus; cc, corpus callosum. (**D**) Higher magnification of M1 shows dense labeling of layer V neurons with GFP. Abbreviations: M1, primary motor cortex; M2, sensorimotor cortex; Caud, caudate;

Put, putamen; G. Pal., globus pallidus; Thal, thalamus; ZI/SZI, zona incerta/subIncerta; STN, subthalamic n.; PAG, periaquadactal grey; APT, anterior pretectal n.; Pont., pontine n.; PPT, pedunculopontine tegmental n.; LRN, lateral reticular n.; Cun, cuneatus n.; GFT, gigantocellular tegmental field ; Cs/MS, superior colliculus / mesencephalic nucleus; c, contralateral; i, ipsilateral Scale bars: B, 2mm; C, 200μm.

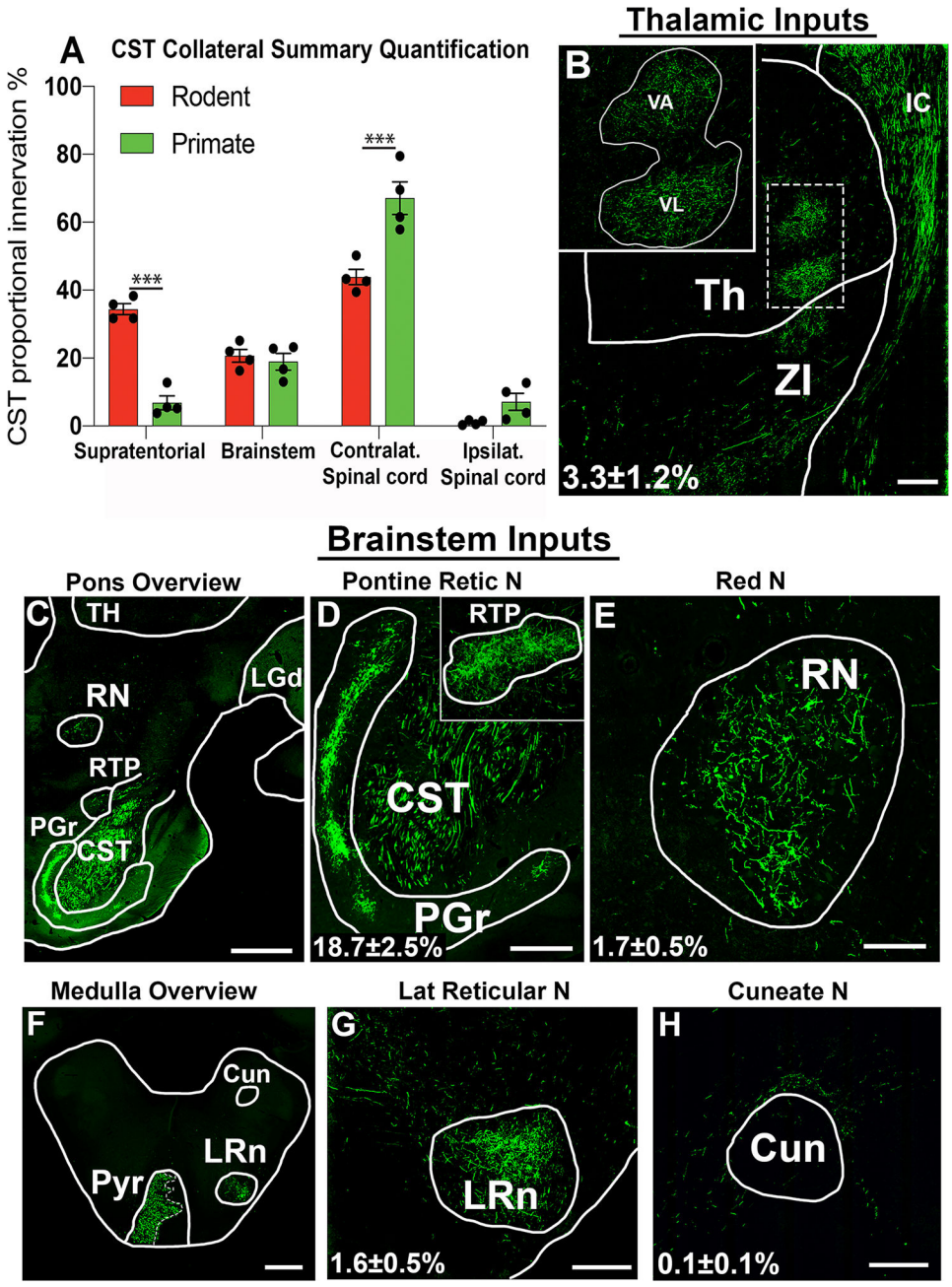

Figure 5: Summary of Corticospinal Quantification and Examples of Distal Forelimb-Controlling Corticospinal Axon Collateral Projections to Brain Regions in the Macaque

(**A**) Corticospinal collateral innervation summary shows extensive corticospinal innervation in supratentorial targets in the rat compared to the macaque ($t_{6,10.65}$ = unpaired t-test, $p<0.0001$, two-tailed); similar brainstem innervation in the two species; and greater spinal cord innervation in the macaque both contralateral and ipsilateral to hemisphere of origin (t_6, 4.38 = unpaired t-test, $p<0.05$, two-tailed). Contralateral (Contralat.), Ipsilateral (Ipsilat.). (**B**) Corticospinal input to the thalamus is found in the ventro-anterior (VA) and ventro-lateral nuclei (inset), two motor relay nuclei that have few inputs in the rat (Supp. Fig 2). Sparse terminals are also present in the zona incerta (ZI). Axons of passage are visible

in the internal capsule (IC). The presence of synapses on corticospinal axons projecting to these target nuclei was confirmed by synaptophysin co-localization (Supp. Fig 8). (**C**) Overview of the pons, showing the corticospinal tract (CST) surrounded by gray matter targets in the pontine gray (PGr), reticulopontine tegmental nucleus (RTP) and red nucleus (RN). TH, thalamus; LGd, dorsal lateral geniculate nucleus. (**D**) Pontine targets are shown at higher magnification, together with axons of passage of the corticospinal tract. (**E**) Axon collaterals projecting to red nucleus. (**F**) Medullary overview: the pyramidal tract (Pyr) is visible together with terminals in the Lateral Reticular nucleus (LRn), shown at higher magnification in (**G**). (**H**) In distinction to the rat, which received dense corticospinal axon collateral input, the Cuneate nucleus (Cun) in the macaque is nearly devoid of corticospinal innervation. Scale bars: C, F; 2mm, B; 1mm; D; 600μm, E; 250μm, G; 150μm,

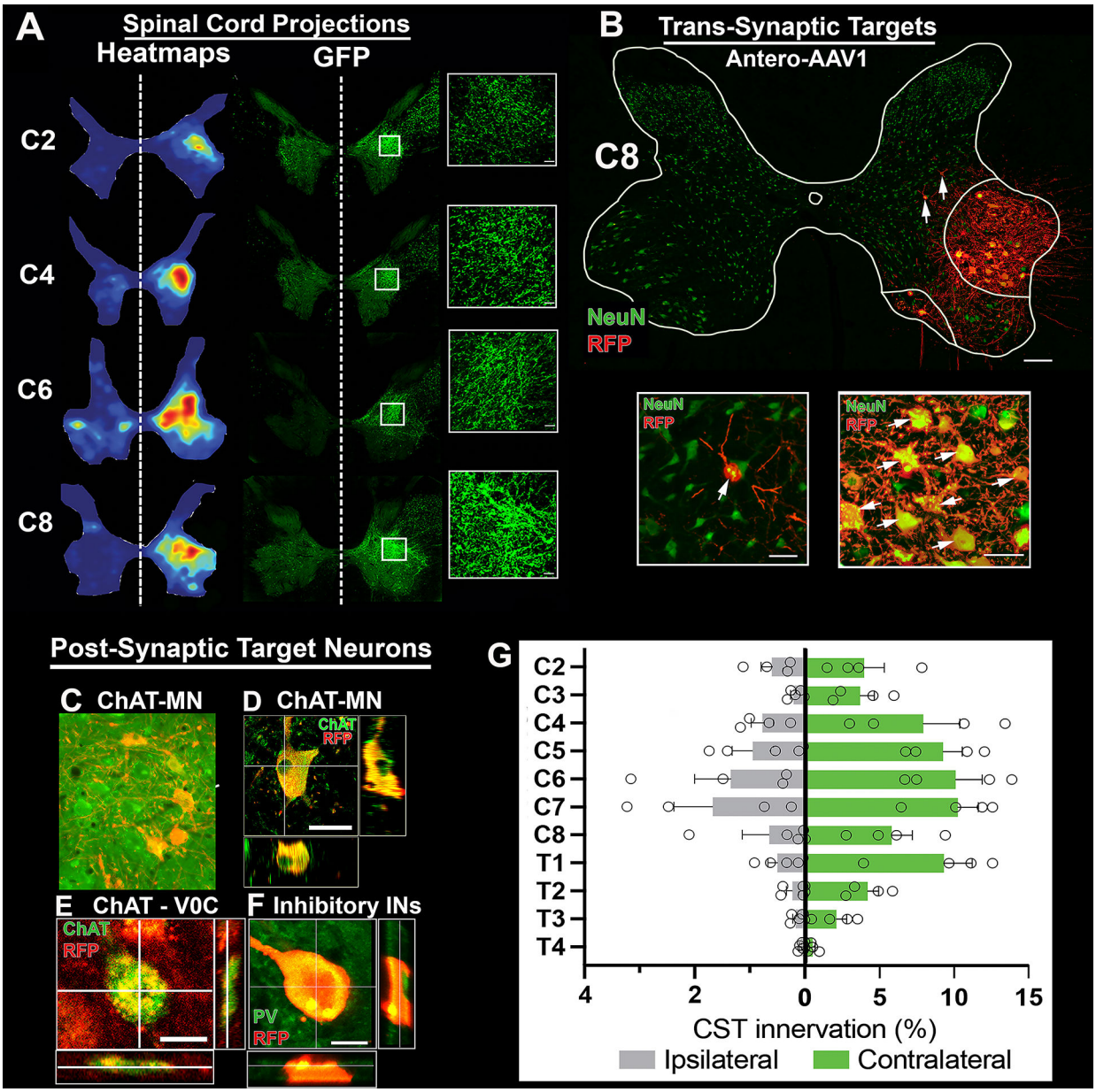

Figure 6: Corticospinal Projections and Post-Synaptic Targets in the Rhesus Macaque Spinal Cord

(**A**) Corticospinal terminal zones throughout the cervical spinal cord after intersectional mapping initiated from forelimb-controlling spinal segments C7-T1. The preponderance of axon terminals are located in caudal cervical segments, in contrast to the rat. (**B**) Spinal cord anterograde monosynaptic targets were identified using trans-synaptic spread of AAV1-Cre injections into M1 and AAVdj-cre-dependent Td-Tomato injections into spinal cord segments C7-T1. 80.5 ± 6.2% of corticospinal projections form monosynaptic projections onto alpha motoneurons and 19.5 ± 6.2% onto spinal interneurons. (**C**) Higher magnification of interneuronal monosynaptic targets of corticospinal axons related to hand control. Cell type-specific markers identify monosynaptic partners of corticospinal axons, including (**D, E**) ChAT-expressing alpha motor neurons (arrows) in lamina IX, (**F**) ChAT-expressing V0c

interneurons in lamina VIII, and (**G**) Parvalbumin (PV) - labeled inhibitory interneurons in lamina VIII. Additional images in suppl. figures 4 and 9. (**H**) Quantification of corticospinal innervation of spinal cord segments C2-T4 as a propostion of their entire CNS projectome. Scale bars: B, 1mm, 180μm, 50 μm; D, E, 50 μm; F, G, 10μm.

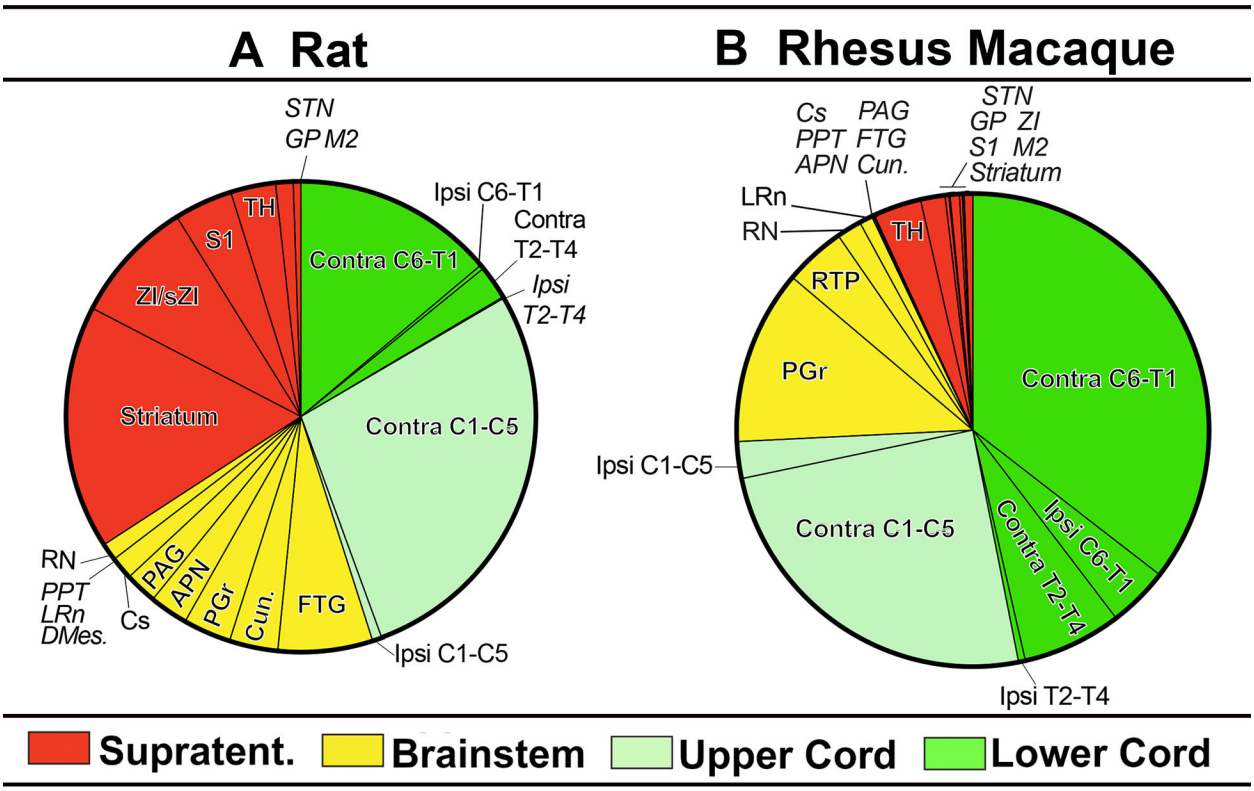

Figure 7: Rat vs. Macaque Summary of Total Corticospinal Proportional Innervation

(**A**) Distribution of all corticospinal innervation in the rat neuraxis. Remarkably, only 13.8% of overall corticospinal axonal output (arising from C7-T1-projecting cortical neurons) terminates in the C6-T1 spinal cord, and another 31% terminates in *upper* cervical segments (C1-C5). The remainder of corticospinal axonal output associated with distal forelimb control terminates in the brain. (**B**) Distribution of all corticospinal projections in the macaque neuraxis. In contrast to the rat, the vast majority of projections access the spinal cord, and particularly the lower cervical spinal cord. Abbreviations: M1, Primary motor cortex; ACA, anterior commissure; M2, sensorimotor cortex; Str, striatum; GP, globus pallidus; SFi, septofimbrial nucleus; ic, Internal capsule; cc, corpus colosum; LV, left ventricle; InG, intermediate gray layer of the superior colliculus; Th, thalamus; ZI, zona incerta; APT, anterior pretectal nucleus; PGr, pontine nucleus; Red, red nucleus; Cs, superior colliculus; PAG, periaqueductal grey; Cun, cuneate nucleus; FTG, gigantotegmental field.

Key resources table

REAGENT or RESOURCE	SOURCE	IDENTIFIER
Antibodies		
RFP	AbCam	Cat# 73 34771
Chicken GFP	Aves	Cat# GFP1020
Rabbit RFP	Rockland	Cat# 601-401-379
Rabbit Ap2b	Santa Cruz Biotechnology	Cat#
Mouse NeuN	Encore	Cat# MLA1B7
Sheep ChoxlO	Abeam	Cat#
Goat ChAT	Genetex	Cat#
Goat Satbl	Santa Cruz Biotechnology	Cat#
Mouse Synaptophysin (SYN)	Novus bio	Cat#
Bacterial and Virus Strains		
AAV9-CAMKII-Cre-SV40	Penn Vector Core	AV-9-PV2396
AAVD J-CAG-FLEX-ArchT-tdT omato	Salk Institute GT3 core	N/A
Cre-dependent HSV-H129ΔTK-tdTomato	see Lo and Anderson, Neuron 2011; 72(6): 938–50	N/A
HSV-H129ΔTK-tdTomato	CNNV, Princeton	N/A
pAAV-hSyn 1-ddCre		
AWD J-FLEX-ArchT-TdT omato		
AAV8-FLEX-ChR2-GFP	UNC Vector Core	
AAVdi-CAG-DIO-gCOMET	Salk Institute GT3 core	
AAVrg-pmSyn1-EBFP-Cre	Salk Institute GT3 core	
AWD J-FLEX-ArchT-TdTomato		
pAAV-hSyn 1-ddCre		
Chemicals, Peptides, and Recombinant Proteins		
Trimethoprim (TMP)		Cat#
Experimental Models: Organisms/Strains		
Rat: Fisher 344 (F344/NHsd)	Envigo	N/A
Rhesus macaques (Macaca mulatta)	See Rosenzweig et al, Nat. Med. 2018; 24:484–490	N/A
Software and Algorithms		
I mage J	Schneider et al., 2012	https://imagej.nih.gov/ii/
Imaris		